Aquaculture 598 (2025) 741952

Contents lists available at ScienceDirect

Aquaculture

journal homepage: www.elsevier.com/locate/aquaculture

The key role of *tyrosinase* in color variation of the autotetraploid *Carassius auratus*

Xi-Dan Xu [a,d], Wan-Jing Peng [a], Yue Zhou [a], Chong-Qing Wang [a], Kun Zhang [a], Xu Huang [a], Xiao-Wei Xu [a], Jin-Hai Bai [a], Ling Xiong [a], Zheng-Kun Liu [a], Xin-Yi Deng [a], Yan Tang [a], Ming Ma [d], Qin-Bo Qin [a,b,c,*], Shao-Jun Liu [a,*]

[a] *State Key Laboratory of Developmental Biology of Freshwater Fish, Engineering Research Center of Polyploid Fish Reproduction and Breeding of the State Education Ministry, College of Life Sciences, Hunan Normal University, Changsha, Hunan 410081, China*
[b] *Nansha-South China Agricultural University Fishery Research Institute, Guangzhou 511458, China*
[c] *Hunan Yuelu Mountain Science and Technology Co.Ltd. for Aquatic Breeding, Changsha, Hunan 410081, China*
[d] *Key Laboratory of Chemical Biology and Traditional Chinese Medicine Research (Ministry of Education), College of Chemistry and Chemical Engineering, Hunan Normal University, Changsha, Hunan 410081, China*

ARTICLE INFO

Keywords:
Autopolyploidization
Tyr
Cooperative regulation
Evolutionary process

ABSTRACT

The autotetraploid *Carassius auratus* (4nRR, 4n = 200, RRRR, brownish-yellow coloration), derived from the whole-genome duplication of *Carassius auratus* red var. (RCC, 2n = 100, RR, red), is a model for understanding the genetics and evolution of polyploid animals. In this study, changes in melanophore and melanin contents indicated differences in melanin metabolism among these two fish species. *Tyrosinase* (*tyr*), a key enzyme in melanin biosynthesis, exhibited significant up-regulation in 4nRR, but its role in pigmentation and coloration variation in 4nRR is unknown. Here, color-variant RCC, 4nRR, and their gynogenetic offspring were established and investigated, revealing that 4nRR *tyr* differentiated from RCC *tyr* to achieve the effective regulation of 4nRR pigmentation. In RCC, two *tyr* homeologs have sub-functionalized to synergistically regulate melanogenesis. Furthermore, color variation was tracked at different developmental stages in mutants. Subsequently, four divergent *tyr* homeologs in 4nRR were localized to four homeologous chromosomes and exhibited predominantly biased expression. Remarkably, yellowish coloration was determined by deficiency of four *tyr* homeologs rather than single or multiple mutated (<4) homeologs. Further, efficient compensatory regulation was confirmed in mutants, suggesting that all *tyr* have evolved to cooperatively regulate 4nRR melanogenesis following autopolyploidization. Notably, numerous homozygous gynogenetic offspring were rapidly constructed with stable coloration traits, further demonstrating the regulatory role of *tyr* homeologs in 4nRR coloration variation, which will enable better generation of novel or tailored strains. These observations reveal a key mechanism underlying coloration formation and variation in 4nRR, while informing skin color–based genetic breeding of polyploid fishes.

1. Introduction

Whole-genome duplication (WGD) or polyploidization is a driver of both evolutionary innovations and ecological adaptations (Otto, 2007; Song et al., 2012; Soltis et al., 2003; Van de Peer et al., 2017). During polyploidization, neopolyploids that form through genome duplication may initially undergo "genomic shock" between divergent subgenomes and eventually evolve into new diploids or paleopolyploids through rediploidization and differentiation (Otto, 2007; Kassahn et al., 2009; Session et al., 2016; Liu et al., 2016; McClintock, 1984). Fish-specific genome duplication (FSGD or 3R) has been proposed to have occurred in the ancestors of teleost fish (Ohno, 1970; Amores et al., 1998; Meyer and Van de Peer, 2005). Further, polyploidy has repeatedly occurred in some taxonomic fish orders. For example, a tetraploidy event involving an additional specific round of genome duplication (s4R) occurred in the ancestor of rainbow trout (*Oncorhynchus mykiss*) (Berthelot et al., 2014), common carp (*Cyprinus carpio*) (Xu et al., 2014; Xu et al., 2019b), and goldfish (*Carassius auratus* red var.) (Luo et al., 2020). In addition, the

* Corresponding authors at: State Key Laboratory of Developmental Biology of Freshwater Fish, Engineering Research Center of Polyploid Fish Reproduction and Breeding of the State Education Ministry, College of Life Sciences, Hunan Normal University, Changsha 410081, Hunan, China.

https://doi.org/10.1016/j.aquaculture.2024.741952
Received 20 September 2024; Received in revised form 10 November 2024; Accepted 25 November 2024
Available online 2 December 2024

amphidiploid *Carassius auratus* red var. (RCC, 2n = 100) is thought to have originated from the interspecific hybridization of two diploids and exhibits meiotic paring and disomic inheritance (Luo et al., 2014; Ma et al., 2014). This allotetraploid species exhibits a unique strategy for balancing subgenomic stabilization and diversification (Luo et al., 2020). Importantly, polyploid breeding can generate remarkable economic and social benefits, as documented in the wide application in various plants and some animals (Awan et al., 2022; Chen et al., 2020; Corneillie et al., 2019; Hu et al., 2020; Wang et al., 2020a). During polyploid breeding, genome restructuring and wide reorganization of gene expression can occur after genomic merging and doubling that is accompanied by alterations and innovations in biological traits.

The autotetraploid *Carassius auratus* (4nRR, 4n = 200, RRRR), originated from a distant hybridization of *Carassius auratus* red var. (RCC, 2n = 100) (♀) × *Megalobrama amblycephala* (BSB, 2n = 48, RR) (♂), and exhibits stable genetic and biological characteristics, leading to the formation of the autotetraploid line (F_1–F_{19}) (Qin et al., 2014). 4nRR individuals possess four sets of RCC-derived chromosomes, resulting from the WGD of diploid RCC. Further, rapid genomic structural changes, regulation of DNA methylation, transcriptome alterations and asymmetric evolution between A and A' homeologous genomes have occurred in the 4nRR genome during polyploidization (unpublished data). Notable divergences in morphological traits have been observed between genotype states, and especially via pigmentation differences, where the diploid RCC fish is red, while 4nRR fish have consistent brownish-yellow coloration. Consequently, this autotetraploid species with a clear genetic background has been considered an exemplary model organism for understanding evolutionary genetics subsequent to WGD events.

The functional diversification of pigment genes following gene duplication during FSGD events is a potential factor that contributes to the diversity and complexity of teleost pigment phenotypes (Braasch et al., 2007, 2009; Meyer and Van de Peer, 2005). *tyrosinase* (*tyr*) is a member of the tyrosinase family, and is an important contributor to melanin biosynthesis in various species (Oetting et al., 1998; Wang et al., 2013; Wang et al., 2014; Wang et al., 2015). FSGD led to the generation of two *tyr* (*tyra* and *tyrb*) from an ancestral *tyr*. The functional divergence has been confirmed in certain fish species. For example, in zebrafish (*Danio rerio*), *tyrb* was lost during the evolution (Braasch et al., 2009). In contrast, *tyrb* was duplicated from *tyra* following the s4R event in rainbow trout and common carp, with both *tyr* genes cooperatively regulating the melanin synthesis and distribution (Boonanuntanasarn et al., 2004; Xu et al., 2022). Previous studies have also demonstrated that the majority of genes in 4nRR fish have twice as many homologs as in RCC fish (Wang et al., 2020b, 2021; Huang et al., 2020; Qin et al., 2019b). Further, some of duplicated homeologs exhibit functional divergence (Xu et al., 2024). Studies of *tyr* have predominantly focused on diploid and natural polyploid animals, with no studies reporting the regulatory mechanisms of *tyr* genes underlying coloration variation in autotetraploid fish, and especially those with a clear genetic background. In this study, RCC and 4nRR were used as model systems to determine the regulatory and functional mechanisms of *tyr* genes underlying coloration formation and variation in 4nRR. Specifically, investigations of cellular biology, pigment compositions, differentially expressed genes (DEGs), functionalities, and artificial gynogenesis were combined to understand *tyr* characteristics. The results of this study advance our understanding of the molecular mechanisms underlying pigmentation and coloration variations in 4nRR, while also providing insights into the genetic and evolutionary processes driving trait variation in autopolyploid animals.

2. Materials and methods

2.1. Experimental fish and tissues

RCC and 4nRR fish used in this study were sourced from the State Key Laboratory of Developmental Biology of Freshwater Fish at Hunan Normal University, China. Experiment animals were raised in the same open-air environment with sufficient sunlight. Given that RCC is characterized by temporal skin color changes, wildtype RCC can be categorized into four distinct skin color periods, each denoted by noticeable coloration stages, including gray coloration (abbreviated as GC), variable-coloration including black and orange regions (VB and VO, respectively), Orange-yellow coloration (OY) and red coloration (RC). In contrast, wild-type 4nRR fish consistently exhibit a brownish-yellow coloration (abbreviated as BY), and was collected at 6 months (abbreviated as 6-BY) and 12 months of age (abbreviated as 12-BY).

Similar phenotypes among the two types of *tyr* single-mutated RCC, were observed during different developmental stages, with each exhibiting unique color variation. During the first developmental stage (I) (within 60 days post-hatching (dph)), mutant individuals displayed light-black streaks or patches (identified as SM-LB) within an off-white color (SM-OW). In the second developmental stage (II) (between 60 and 110 dph), the skin transitioned to light yellow hue (SM-LY) adorned with deep black streaks or patches (SM-DB). Finally, by the third stage (III) (beyond 110 dph), the entire fish's body exhibited a red coloration, wherein the regions of red skin originating from the SM-LY and SM-DB were identified as SM-WR1 and SM-WR2, respectively. Similarly, the *tyra* and *tyrb* double mutant RCC individuals that were established by simultaneously disrupting two *tyr* homeologs manifested a transition in skin coloration, shifting progressively from an initial off-white hue (DM-OW) to an intermediate stage of yellowish (DM-Y), then orange-yellow (DM-OY), and ultimately the red (DM-WR) pigmentation. However, the coloration characteristics of four distinct types of *tyr* single-mutated 4nRR were unaffected, consistently presenting a brownish-yellow coloration and referred to as SM-BY. In contrast, simultaneous knockout of four *tyr* genes resulted in the emergence of two phenotypes, with complete mutants exhibiting pervasive melanin deficiencies with yellowish body surfaces (designated as M-Y), while chimeric mutants retained melanin in partial skin regions (i.e., Shallow black, designated as M-SB).

The aforementioned skin tissues were used for transcriptional expression analysis of genes and observations of chromatophores. All procedures conducted in this study rigorously adhered to the ethical requirements of the Institute of Experimental Animals, Hunan Province, China. All fish were deeply anesthetized using 100 mg/L MS-222 (E10521, Sigma-Aldrich, St Louis, MO, USA) before surgically removing tissue.

2.2. Determination of fish melanin contents

Five individuals were sampled from each of the 12-month-old wild-type RCC (red coloration) and 4nRR groups. Skin tissues weighing 70 mg were collected from the upper regions of the fish lateral lines. Skin tissue homogenates were prepared using 1 mL PBS or saline, followed by the removal of particulates through centrifugation at approximately 3000 ×*g* for 10 min. The resulting tissue fluid was either immediately subjected to assays or aliquoted and stored at −20 °C or − 80 °C for future analysis. Skin melanin contents were quantified using fish melanin enzyme-linked immunosorbent assay (ELISA) (ZK-08158, Shanghai Enzyme-linked Biotechnology Co., Ltd., China) in accordance with the manufacturer's instructions. Absorbances were measured at 450 nm using a spectrophotometer.

2.3. Chromatophore observations

The identification of chromatophores within the skin of both wild-type and mutant individuals was conducted via frozen sectioning and transmission electron microscopy (TEM). Skin samples were collected and preserved at 4 °C, along with a portion of subcutaneous muscle tissues. Pigment cells were observed with light microscopy and confirmed via fresh skin pieces that were promptly soaked and fixed in 4

% paraformaldehyde solution for 12 h, embedded in tissue OCT-freeze medium, and then rapidly froze in liquid nitrogen. Section with thickness of 5 μm were obtained using a Leica CM3050S Frozen Microtome and comprehensively visualized using the Leica DM2500. Skins were subsequently reexamined using TEM to differentiate pigment cells and its ultrastructures. Skin pieces were fixed with 2.5 % glutaraldehyde at 4 °C for 12 h, treated with 2 % OsO4 for 2 h, and then washed with PBS. Tissues then were subjected to dehydration using an ethanol gradient series, specimens were embedded in epoxy resin, sectioned, and then stained with uranyl acetate either for 2 h or overnight. The specimens were viewed using a cover slip and with a Hitachi TEM system.

2.4. Comparative analysis of skin transcriptomes and identification of key genes involved in melanin-based coloration

Three biological replicates were performed each for red RCC and brownish-yellow 4nRR skin transcriptomic analysis, as previously described (Xu et al., 2024). The quantities and qualities of total extracted RNA were assessed using a NanoDrop-2000 spectrophotometer (Thermo Scientific, USA) and agarose (1.0 %) gel electrophoresis. cDNA synthesis, library construction (three each for RCC and 4nRR fish, TruSeq™ RNA Library Prep Kit, Illumina, USA), library sequencing, alignment to the reference genome (i.e., the 4nRR reference genome, in NCBI under the accession PRJNA1138278, unpublished, STAR software), and bioinformatics analysis were conducted at Beijing Biomarker, China, as previously described (Anders and Huber, 2010; Gotz et al., 2008; Li et al., 2009). The transcription levels of genes were quantified based on the Fragments Per Kilobase Million (FPKM) metric in the StringTie program (v.1.3.4d) and thereafter normalized using the Deseq2 R package (v.1.26.0). Genes displaying a fold change ≥ 2 and a false discovery rate (FDR) < 0.05 were identified as differentially expressed genes (DEGs). GO and KEGG enrichment analyses of DEGs were performed using the clusterProfiler R package (v.3.14.0). DEGs were identified as key genes involved in melanin-based coloration based on the chromatophore, pigment, and transcriptomic comparisons between RCC and 4nRR individuals. The DEGs were further verified using quantitative real time PCR (qPCR).

2.5. Gene identification and sequence analysis

Total RNAs from all samples were extracted using the Trizol protocol (15,596,026, Thermo Scientific, USA), followed by assessment of quality and concentration using a NanoDrop-2000 spectrophotometer and agarose (1.0 %) gel electrophoresis. cDNAs were synthesized using the SMARTerTM PCR cDNA Synthesis Kit (634,926, Clontech, Mountain View, CA, United States) following the manufacturer's instructions. The *tyr* gene sequence was derived using cDNA and DNA from skin samples as templates. Two homeologs of *tyr* and four homeologs of *tyr* were respectively cloned from RCC and 4nRR samples utilizing a homology-based cloning strategy, and have been deposited in GenBank (OP466737 and OP466738 in RCC, OP466739 to OP466742 in 4nRR). The cDNA and DNA amplification primers were designed based on the genome sequences of RCC (ASM336829v1) and 4nRR (In NCBI under the accession PRJNA1138278, unpublished) (Supplementary Table S1). Given that the divergent *tyr* homeologs exhibited differences in their nucleotide sequences, four unique pairs of primers were designed in the regions where the start codon and stop codon are located, to specifically amplify the CDS regions of *tyra*, *tyrb*, *tyrc*, and *tyrd*, respectively. DNA amplification primers were then designed to specifically amplify the DNA sequences of *tyra* and *tyrb* in RCC, and *tyra*, *tyrb*, *tyrc*, and *tyrd* in 4nRR, based on specific SNPs present among the reference homeologs. Due to the high nucleotide sequence identity among divergent *tyr* homeologs in both fish species, PCR amplification products were purified, and subsequently subcloned into DH5α competent cells, and sequenced to acquire and distinguish the specific sequence of *tyr* homeologs present in both RCC and 4nRR. Multiple amino acid sequence alignments and phylogenetic analyses were conducted using the DNAMAN (v.7.0) and Molecular Evolutionary Genetics Analysis (MEGA 7) programs, respectively (Kumar et al., 2016). The amino acid sequences of *tyr* obtained from various species were retrieved from the GenBank or Ensemble databases, including *Cyprinus carpio* var. *color* (*tyr1*: AQX36322.1, *tyr2*: XP_018952990.2), *Bufo bufo* (CAR95491.1), *Danio rerio* (AAN17339.1), *Gallus gallus* (AAB36375.1), *Homo sapiens* (AGV39054.1), *Mus musculus* (AAA37806.1), *Oncorhynchus mykiss* (*tyr1*: NP_001117691.1, *tyr2*: NP_001117694.1), *Takifugu rubripes* (XP_003968377.3), *Oryzias latipes* (NP_001098272.1), *Salmo salar* (NP_001117115.1), *Ictalurus punctatus* (NP_001187014.1), *Oreochromis niloticus* (XP_003441635.1), *Oryzias celebensis* (UBR18743.1), *Rhinatrema bivittatum* (XP_029457566.1), *Patagioenas fasciata monilis* (OPJ89948.1), *Siniperca chuatsi* (XP_044059474.1), and *Bagarius yarrelli* (TSX58275.1).

2.6. qPCR analysis

The qPCR was conducted on the QuantStudio™ 5 Real-Time PCR Instrument (Thermo Fisher Scientific), as previously described (Wang et al., 2021). Both RCC and 4nRR samples were analyzed in triplicate. Specific amplification primers used for each *tyr* homeolog are shown in Supplementary Table S1, with *β-actin* and *18S* used as internal reference genes. Relative expression levels were calculated using the $2^{-\Delta\Delta Ct}$ method (Livak and Schmittgen, 2001) and the reference gene expression data was derived from the geometric mean expression of the two genes. All the data were expressed as the mean + standard error (SE). Statistical significance was evaluated by one-way analysis of variance (ANOVA) and the test of Tukey to determine the significance of different research groups. Given that divergent *tyr* homeologs exhibited differences in their nucleotide sequences, two and four unique pairs of primers were designed for RCC and 4nRR amplifications, respectively. The primers were used to specifically amplify RCC-*tyra*, RCC-*tyrb*, 4nRR-*tyra*, 4nRR-*tyrb*, 4nRR-*tyrc*, and 4nRR-*tyrd*. Primers were designed to match differences in the coding sequence (CDS) regions of the homeologs. To further determinate the amplification specificity achieved by the primers, qPCR products generated by amplification from skin tissue templates ($n = 3$ fishes) were subjected to purification, cloning, and sequencing, with analysis of each primer pair amplicons. From each sample, 30–32 clones were selected for sequencing and characterization based on specific SNPs present among homeologs.

2.7. Establishment of tyr-mutated RCC and 4nRR with CRISPR/Cas9

Single and multiple-mutated *tyr* from RCC and 4nRR were generated utilizing the CRISPR/Cas9 system. The sgRNA target sites were first designed on the first exon by strategically aiming to disrupt the critical domains, including the epidermal growth factor (EGF)-like domain, transmembrane domain, and copper binding sites, that were determined through the online design program (http://crispr.mit.edu/,http://zifit.partners.org/ZiFiT/CSquare9Nuclease.aspx). The sgRNAs (four for *tyra*, two for *tyrb*, four for *tyrc*, and three for *tyrd*) were transcribed with the RiboMAXTM Large Scale RNA Production System-T7 (P1300, Pomega, USA) (Supplementary Table S2), and their integrity was subsequently tested through agarose gel electrophoresis. The nls-Cas9-nls protein was sourced from the NEB Company (M0646M, NEB, USA). Mixtures of in vitro-synthetic sgRNAs (150–200 ng/μL) that were prepared within one month, and cas9 protein (20 pmol/μL), were co-injected into one-cell stage embryos. The injection volumes for both RCC and 4nRR embryos were equivalent to 1/8 of the zygote volume. *Tyra*-mutated, *tyrb*-mutated, and *tyra-tyrb*-mutated RCC were successfully produced. Four types of single *tyr*-mutated F_0 individuals were generated in 4nRR fish. In addition, the establishment of *tyra-tyrb*-mutated, *tyra-tyrc*-mutated, *tyra-tyrd*-mutated, *tyrb-tyrc*-mutated, *tyrb-tyrd*-mutated, *tyrc-tyrd*-mutated, *tyra-tyrb-tyrc*-mutated, *tyra-tyrb-tyrd*-mutated, *tyrb-tyrc-tyrd*-mutated, *tyra-tyrc-tyrd*-mutated, and *tyra-tyrb-*

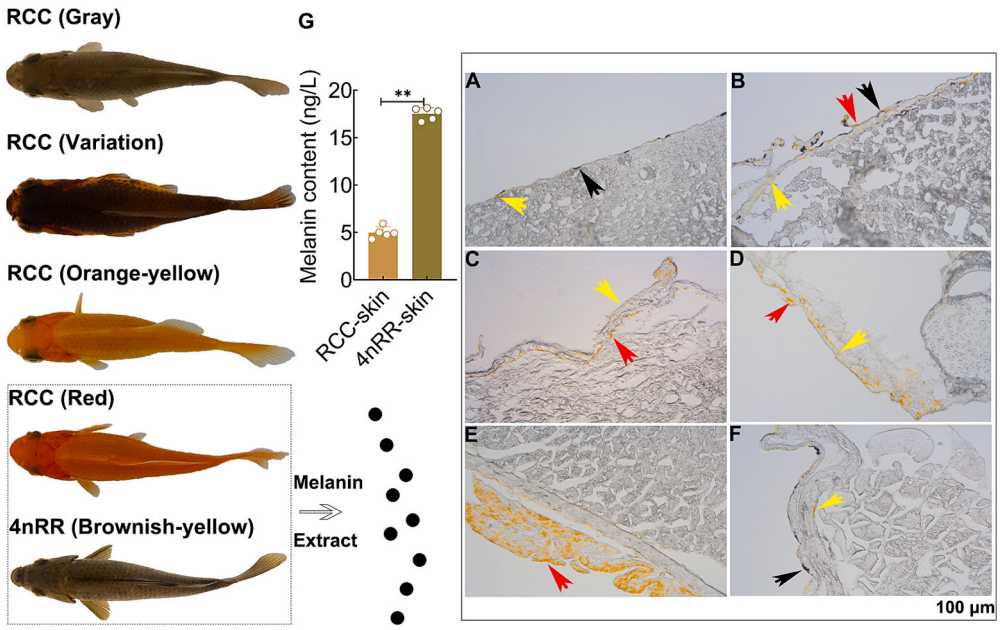

Fig. 1. Identification of pigment cells and melanin in RCC and 4nRR fish skins. A–F, Composition and distribution of pigment cells in GC (A), VB (B), VO (C), OY (D), and RC (E) stages of RCC, and in 6-month-old and 12-month-old 4nRR (F). GC: gray coloration stage; VB: black coloration in variable-coloration stage; VO: orange coloration in variable-coloration stage; OY: orange-yellow coloration stage; RC: red coloration stage. The red, black, and yellow arrows indicate erythrophores, melanophores, and xanthophores, respectively. G, Melanin content in the RC stages of RCC and 12-month-old 4nRR based on ELISA assays ($n = 5$ fishes). Each point represents the mean of three technical replicates from each fish. Scale bars are shown at the bottom-right corners of the images. Asterisks indicate statistically significant differences; **, $P < 0.01$. (For interpretation of the references to color in this figure legend, the reader is referred to the web version of this article.)

tyrc-tyrd-mutated 4nRR mutants were generated. Consequently, three and fifteen types of mutants were obtained for RCC and 4nRR fish, respectively. Thirty-six hours after microinjection, PCR amplification and sequencing of *tyr* target regions was conducted using DNA extracted from 30 randomly selected embryos. The editing efficiency was initially verified by overlapping peaks. Later, adult mutants with different phenotypes (i.e., based on pigmentation and distribution of melanin on body surfaces) were subjected to similar PCR-specific amplifications using blood-derived DNA as templates. The amplicons were subcloned into the pMD19-T vector (6013, TakaRa, Japan) for sequencing and genotyping. At least 24 clones were randomly selected from each genotype mutation sample ($n = 3$ fishes). Phenotypic features of all mutant fish were captured against a white background. The ImageJ software program (Abràmoff et al., 2004) was used to calculate the melanin area in skins of mutant individuals.

2.8. Generation of artificial gynogenetic offspring

F_0 Type I RCC with complete melanin deficiency were selected for artificial gynogenesis to obtain F_1 homozygous mutants. UV irradiation and cold shock were performed to induce genetic inactivation in sperm and chromosome diploidy, respectively. UV-irradiated BSB sperm was then used as a trigger to activate embryogenesis. Briefly, the dilution mixture (milt: D-Hank's solution = 1:10) was evenly spread on a petri dish (20 cm in diameter), and then exposed to UV light. Irradiation times require microscopic monitoring of sperm vitality for 10–20 min, due to variation in sperm viability in different BSB individuals. The F_0 Type I RCC eggs were then fertilized by UV-irradiated sperm at 21 °C and treated by cold shock (0–4 °C) for 30 min at 20 min post-fertilization, resulting in the generation of artificial mitotic gynogenetic offspring.

Previous study indicated that 4nRR females can produce autodiploid eggs (2n = 100) after activation by UV-irradiated BSB sperm, with the autodiploid eggs developing into all-female autodiploid gynogenetic offspring without chromosome doubling treatment (Qin et al., 2018). In 4nRR mutants, individuals with complete melanin defects were chosen to proliferate by gynogenesis to obtain diploid offspring. Generation of diploid offspring was conducted, as previously described (Qin et al., 2018).

2.9. Examination of ploidy

Measurements of DNA content and examination of chromosome numbers were used to confirm ploidy levels in gynogenetic offspring. DNA contents of erythrocytes from RCC, 4nRR, and gynogenetic offspring were measured by collecting the red blood cells from caudal veins. The blood samples were then sequentially treated, filtered, and measured according to previously described method (Qin et al., 2014). In addition, chromosomal preparation was carried out using the kidney tissues of RCC, 4nRR, and gynogenetic offspring at four months of age following a previously described method (Qin et al., 2014). Two-hundred metaphase chromosome spreads (20 spreads per sample) were analyzed for each fish type. The preparations were examined under 3330× magnification with an oil immersion lens.

3. Results

3.1. Composition and distribution of pigment cells in RCC and 4nRR skins at different developmental stages

The composition and distribution of pigment cells in RCC and 4nRR skins were directly observed via frozen sections. Dynamic progression in the composition of pigment cells was observed across the four discernible developmental stages in the RCC fish. Noticeable coloration stages included gray coloration (GC), variable-coloration including black and orange regions (VB and VO, respectively), orange-yellow coloration (OY), and red coloration (RC). In the initial stage, GC, melanophores and xanthophores were evident (Fig. 1A). In the color variation stage, a more complex assemblage of pigment cells emerged in the VB region, comprising melanophores, xanthophores and erythrophores (Fig. 1B), while the VO region exhibited substantial numbers of xanthophores, accompanied by a minor presence of erythrophores (Fig. 1C). A remarkable abundance of erythrophores predominated in the OY stage,

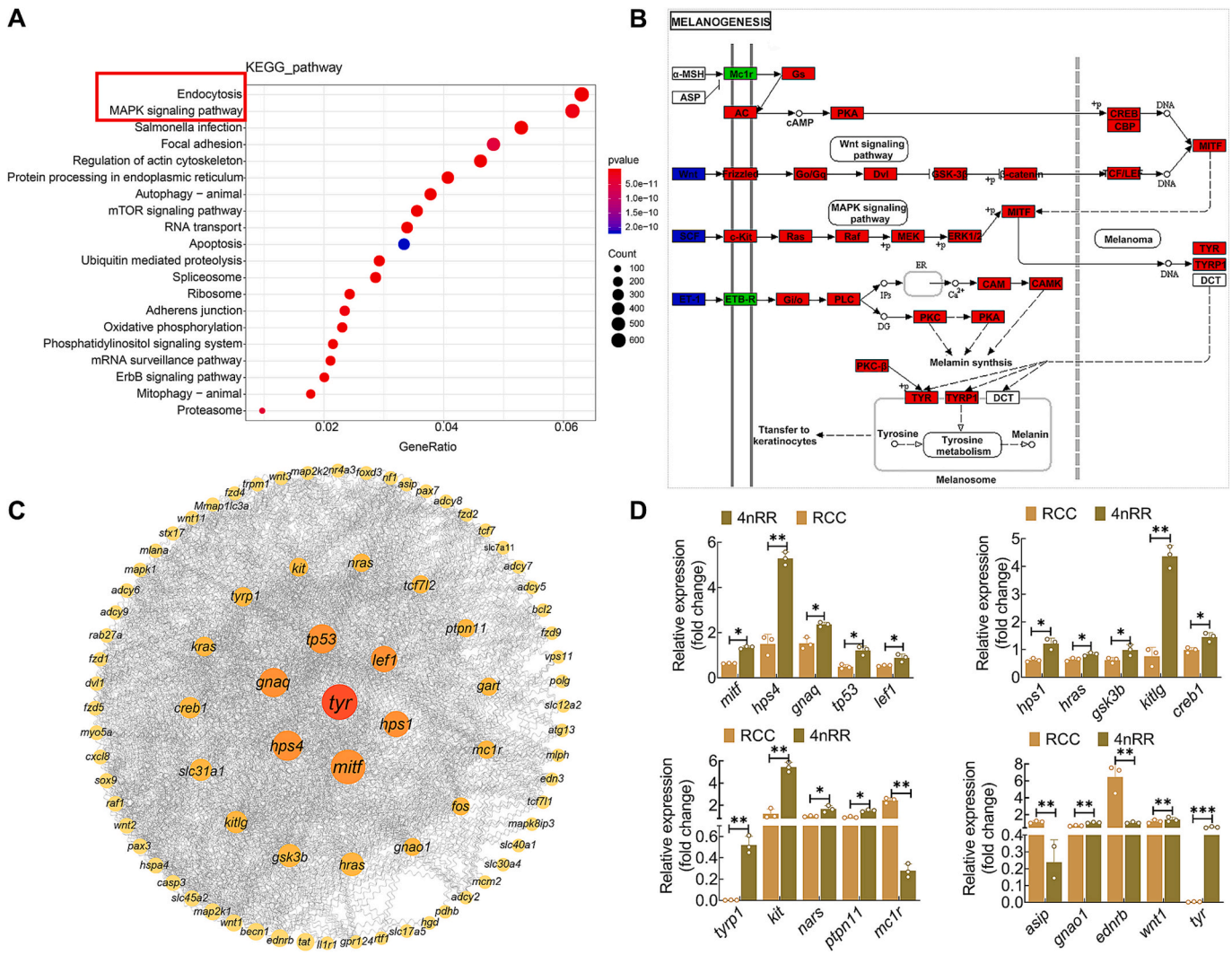

Fig. 2. Identification of key genes involved in melanin-based coloration. A, KEGG pathway enrichment analysis of DEGs. The red box indicates the top two most enriched pathways. B, Expression changes of genes in the melanogenesis pathway (Ko04916). In 4nRR skin, *kit*, *nras*, *raf1*, and *mapk2* were up-regulated genes of the MAPK signaling pathway relative to RCC skins. These genes can further affect the significant up-regulation of *mitf*, *tyr*, and *tyrp1* genes in the melanogenesis pathway of 4nRR. Red and green boxes indicate up-regulated and down-regulated genes, respectively. The symbol "○" designates compounds, while "+p" denotes phosphorylation, "→" indicates activation, and "⇢" represents indirect action. C, Protein-protein interaction network of melanin-based coloration-related genes in RCC and 4nRR groups. D, qPCR verification of key genes. Data represent mean ± (SE), $n = 3$ fishes, with each point representing the mean of three technical replicates from each fish. Statistically significant differences are indicated by asterisks. ns: not significant; *: $P < 0.05$; **: $P < 0.01$; ***: $P < 0.001$. (For interpretation of the references to color in this figure legend, the reader is referred to the web version of this article.)

while xanthophores also persisted (Fig. 1D). Finally, erythrophores were present in adult RCC fish (Fig. 1E). In contrast, 4nRR skins consistently exhibited brownish-yellow coloration and the composition of pigment cells in skins remained the same at 6 and 12 months of age, with melanophores and xanthophores both being present (Fig. 1F). These observations suggest that autotetraploidization significantly altered the pigment cell compositions, endowing 4nRR fish with distinct pigmentation changes compared to the diploid parent.

3.2. Higher melanin content in 4nRR fish

The formation of black/brown skin coloration in fish is thought to be related to melanin in melanophores, while vibrant fluorescent coloration (e.g., red, yellow or orange) is dependent on pteridines/carotenoids deposited within xanthophores and erythrophores. Given the distinct chromatophores observed between 12-month-old red RCC (erythrophores) and brownish-yellow 4nRR (xanthophores, erythrophores, and melanophores), the melanin content of skins from both fish were investigated with ELISA, with all measurements conducted in triplicate ($n = 5$ fishes). The melanin content within 4nRR skin (average of 17.516 ng/L) was significantly higher than in RCC (4.988 ng/L; $P < 0.01$) (Fig. 1G). The observed differences in melanin content indicate that autotetraploidization may induce regulatory changes in melanocortin system that may be involved in the color variation.

3.3. Transcriptome profile comparisons and identification of key genes involved in melanin-based coloration

To investigate the molecular mechanisms underlying coloration formation and variation in 4nRR, skin transcriptomes of RCC and 4nRR (RCC vs. 4nRR) were compared. A large number of DEGs (22,150) were identified among the six transcriptomes, with 20,681 up-regulated and 1469 down-regulated DEGs (Supplementary Table S3). Thus, important functional differences may occur after autotetraploidization.

Gene Ontology (GO) analysis revealed the higher percentages of several GO terms associated with pigment metabolism. For example,

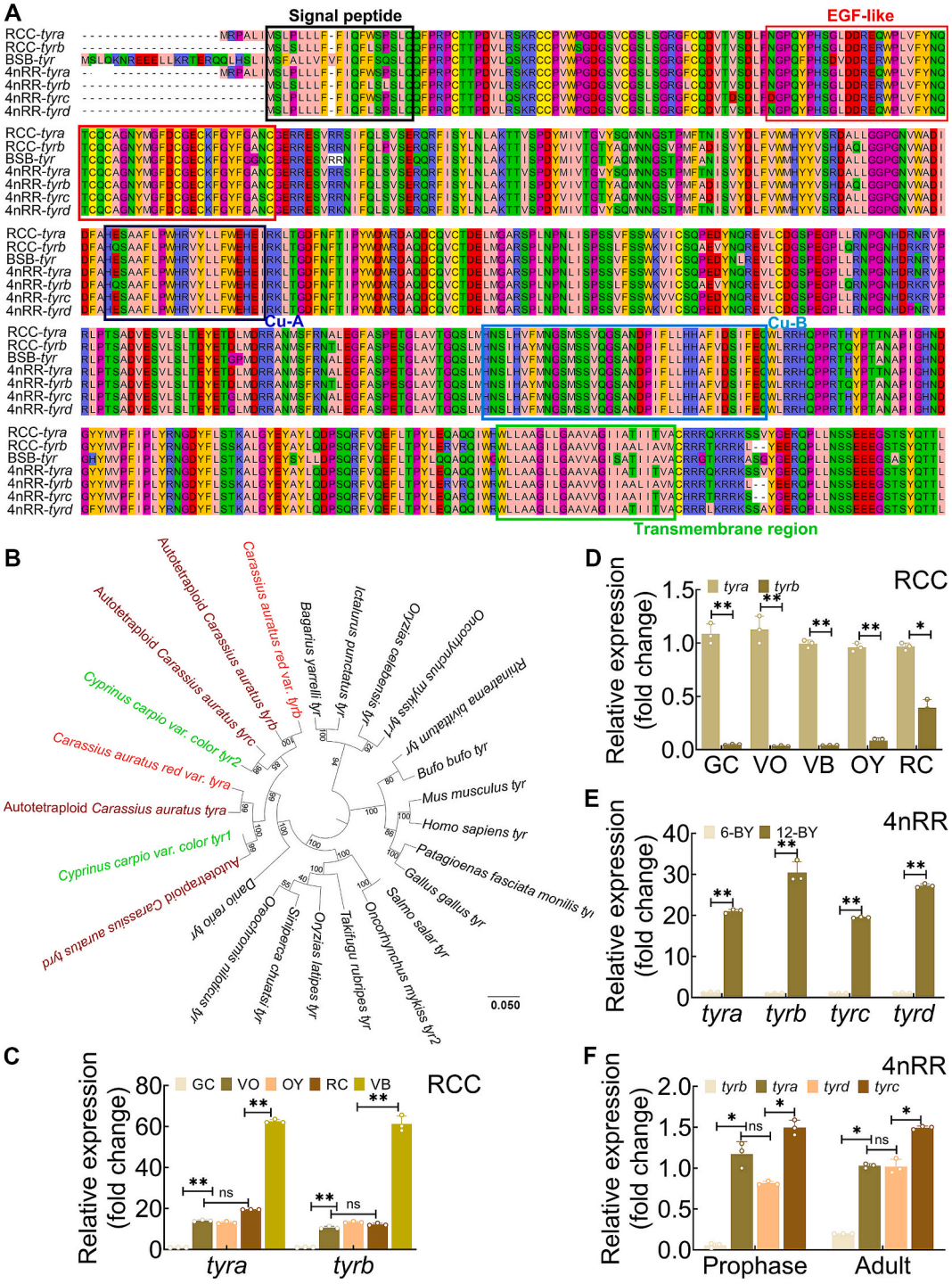

Fig. 3. Identification and expression of *tyr* homeologs in RCC and 4nRR. A, Multiple amino acid alignment of *tyr* homeologs. Consecutive dashes (–) indicate positions of amino acid deletions. B, Phylogenetic analysis of vertebrate *tyr* homologs. Phylogenetic analysis was conducted with the neighbor-joining methods. C—F, Expression of two *tyr* homeologs in RCC (C, D) and four *tyr* homeologs in 4nRR (E, F), n = 3 individuals. Each point represents the mean of three technical replicates from each individual. Asterisks display statistically significant differences. ns, not significant; *, $P < 0.05$; **, $P < 0.01$.

significantly enriched GO terms included "melanin biosynthetic process", "pigmentation", "developmental pigmentation", and "melanosome organization" in the biological process category, "melanosome" in the cellular component category, and "metal ion binding", "oxidoreductase activity", and "copper ion binding" in the molecular function category (Supplementary Tables S4–S6). These functions may be related to the emergence of melanin/melanophores in 4nRR fish. The DEGs were also mapped to 303 Kyoto Encyclopedia of Genes and Genomes (KEGG) pathways, with the 20 most enriched pathways involved in metabolism, genetic information processing, cellular processes, and signal transduction (Fig. 2A). The "endocytosis" pathway, was most enriched and is related to lipid metabolism and transport. The enrichment of this pathway may be associated with dramatic changes in skin carotenoids stored after autotetraploidization, further contributing to the formation of xanthophores in 4nRR and erythrophores in red RCC. Our previous findings also revealed differential expression of genes

associated with carotenoid metabolism between RCC and 4nRR, with relevant genes showing appropriate explainable patterns of up- regulation (*abca1*, *slc19a2*, *pax7*, and *xdh*) or down-regulation (*abcc1*, *apoe*, *slc46a1*, *stard3*, *bco2*, *pax3*, *sox5*, *slc5a6*, *gch1*, *bco1*, and *scarb1*) (Xu et al., 2024). Interestingly, the "MAPK signaling pathway" was second most enriched. In 4nRR skin, *kit* (*KIT proto-oncogene receptor tyrosine kinase*), *nras* (*NRAS proto-oncogene, GTPase*), *raf1* (*Raf-1 proto-oncogene serine/threonine-protein kinase*), and *mapk2* (*mitogen-activated protein kinase kinase 2*) were up-regulated genes of the MAPK signaling pathway relative to RCC skins. These genes can further affect the significant up-regulation of *mitf* (*melanocyte inducing transcription factor*), *tyr*, and *tyrp1* (*tyrosinase related protein 1*) genes in the melanogenesis pathway of 4nRR (Fig. 2B), consistent with the GO-enriched terms. In addition, the tyrosine and Wnt signaling pathways were also enriched among DEGs (Supplementary Fig. S1–S2), where they may significantly contribute to processes related to the formation and differentiation of melanin metabolism. These results indicate that melanin metabolism might change following autotetraploidization, potentially resulting in the presence of melanophores in skins.

Further investigation and global evaluation of the effects of key melanin metabolism genes on coloration variation in 4nRR revealed 96 essential DEGs implicated in melanin-based coloration that were consistent with the above melanin and skin transcriptomic analyses, alongside published results. A protein-protein interaction (PPI) network was constructed using the STRING tool, and candidate key genes was further identified using Cytoscape (Fig. 2C). Interactome reconstructions identified 20 DEGs, with interaction levels >15, that were considered as hub genes. The expression of hub genes was confirmed with qPCR. The results were consistent with the RNA-Seq analyses, with 17 up-regulated and 3 down-regulated genes in the 4nRR group compared to the RCC group (Fig. 2D), highlighting the reliability of the RNA-Seq results. *Tyr* is a pivotal component in melanin biosynthesis and transcriptional validation indicated its significant up-regulation in 4nRR group compared with RCC group ($P < 0.001$). Thus, *tyr* is likely an important contributor to coloration formation and pigmentation variation following autotetraploidization.

3.4. Diversification of four divergent tyr homeologs in 4nRR

Two divergent *tyr* homeologs (RCC-*tyra* and RCC-*tyrb*) were successfully cloned from RCC and localized to Scaffolds 255 and 3026, respectively. In contrast, four distinct *tyr* homeologs were identified in 4nRR (4nRR-*tyra*, 4nRR-*tyrb*, 4nRR-*tyrc*, and 4nRR-*tyrd*) that were localized to chromosomes 29 A, 24 A, 24 B, and 29 B, where 4nRR-*tyra* originated from RCC-*tyra* and the others from duplication events (Fig. 3A). The *tyr* in RCC and 4nRR comprised five exons and four introns, similar to vertebrate *tyr* genes. Further, all of the genes retained the signal peptide, an epidermal growth factor (EGF)-like domain, a transmembrane domain, and two highly conserved copper binding sites (Cu-A and Cu—B) (Fig. 3A; Supplementary Fig. S3). Multiple alignment and analyses revealed nucleotide and amino acid identities between RCC-*tyra* and RCC-*tyrb* of 93.35 % and 91.21 %, respectively. In 4nRR, 4nRR-*tyra* and 4nRR-*tyrb* exhibited 93.16 % nucleotide identity and amino acid identity of 91.4 %. 4nRR-*tyrc* and 4nRR-*tyrd* exhibited 93.66 % nucleotide identity and 93.08 % amino acid identity. Notably, the nucleotide and amino acid identities of RCC-*tyrb* and 4nRR-*tyrb* were 98.94 % and 99.44 %, respectively, with only three amino acid variant sites ($RCC^{tyrb}/4nRR^{tyrb}$, P^{15}/L^{15}, S^{40}/P^{40}, P^{127}/S^{127}). Interestingly, the nucleotide identities of 4nRR-*tyrc* and 4nRR-*tyrd*, with RCC-*tyra* were 93.91 % and 96.33 %, respectively, while the amino acid identities were was 93.08 % and 96.39 %, respectively. In contrast, 4nRR-*tyrc* and 4nRR-*tyrd* exhibited 93.84 % and 91.98 % nucleotide identity with RCC-*tyrb*, respectively, along with 93.25 % and 91.4 % amino acid identities, respectively. Thus, 4nRR-*tyrc* had higher identity with RCC-*tyrb*, while 4nRR-*tyrd* was configured with higher identity with RCC-*tyra* (Fig. 3A; Supplementary Table S7). In addition, syntenic alignments of genomic regions containing *tyr* revealed that homologous gene structures in 4nRR fish were greatly altered in comparison to RCC fish (Supplementary Fig. S4).

Significant mutations in nucleotide sequences were observed in both duplicated 4nRR-*tyrc* and 4nRR-*tyrd* when compared to RCC-*tyra* and RCC-*tyrb*. To further evaluate the origins of amino acid variation within both duplicated 4nRR-*tyrc* and 4nRR-*tyrd*, two *tyr* in RCC and one *tyr* in *Megalobrama amblycephala* (BSB-*tyr*) were used as controls in comparisons. Statistical analysis of variable amino acid sites revealed distinct origins for the variant sites in both 4nRR-*tyrc* and 4nRR-*tyrd*. Notably, 4nRR-*tyrc* predominantly originated from the fusion recombination event of RCC-*tyrb* (11 sites), overlapping regions between RCC-*tyrb* and BSB-*tyr* (8 sites), and endogenous mutations (10 sites). Conversely, 4nRR-*tyrd* primarily derived from the fusion recombination event of RCC-*tyra* (15 sites), overlapping regions between RCC-*tyra* and BSB-*tyr* (27 sites), and endogenous mutations (5 sites) (Fig. 3A; Supplementary Fig. S5). In addition, 4nRR-*tyrc* exhibited one mutation site derived from BSB-*tyr*. The composition of these variable sites indicated that the genesis of 4nRR-*tyrc* was driven by duplication subsequent to hybridization and subsequent variation of RCC-*tyrb*, while 4nRR-*tyrd* was induced by analogous processes involving RCC-*tyra*.

Phylogenetic analysis demonstrated that *tyr* genes were phylogenetically similar, where *tyr* genes in RCC and 4nRR clustered with those from Cyprinidae (Fig. 3B). The homologs RCC-*tya* and RCC-*tyrb* clustered with those of 4nRR-*tyra* and 4nRR-*tyrb*, respectively. In addition, duplicated 4nRR-*tyrc* and 4nRR-*tyrd* were individually clustered with *tyr2* and *tyr1* of *Cyprinus carpio* var. color. The 4nRR-*tyrc* and 4nRR-*tyrd* homeologs were located, on an additional branch that then clustered in association with *tyrb* and *tyra*, respectively. Overall, these homologs clustered with those from *Danio rerio*. The above results indicate that, 4nRR-*tyrc* and 4nRR-*tyrd* originated from the duplication and variation of RCC-*tyrb* and RCC-*tyra*, respectively, following autotetraploidization, implying that these duplicates may be functionally differentiated.

3.5. Differential expression of tyr homeologs

RCC is characterized by temporal changes in skin color, wherein melanophores present on the body surface gradually increase in the GC to VB stages, followed by gradual decreases in the VB to VO and OY stages, all followed by their eventual disappearance in the RC stage. Transcriptional expression of *tyr* within the skins of RCC were analyzed with qPCR. Similar expression patterns were observed for the two *tyr* homeologs. The most pronounced expression levels were detected in VB skins (3.90–5.02-fold-changes vs. VO, OY, and RC skins, $P < 0.01$), followed by VO, OY and RC skins (10.93–14.03-fold-changes vs. GC skins, $P < 0.01$). The lowest expression was observed for GC skins, indicating that both *tyra* and *tyrb* exhibited the highest expression in variation-black skin with abundant melanophores (Fig. 3C). Additionally, *tyra* was significantly more expressed than *tyrb* in all five RCC skin expression assays ($P < 0.01$ in GC, VO, VB; OY, $P < 0.05$ in RC) (Fig. 3D). This observation highlights the differential expression of *tyr* homeologs and their important roles in controlling skin color variation in RCC fish.

4nRR fish coloration is generated from the combination and distribution of melanophores and xanthophores, resulting in the overall presentation of brownish-yellow hues. Four *tyr* homeologs exhibited distinct expression patterns. Among these, 4nRR-*tyrc* exhibited the highest expression, with approximately 1.36- and 1.62- fold higher expression than 4nRR-*tyra* and 4nRR-*tyrd*, respectively ($P < 0.05$). The expression levels of 4nRR-*tyra* and 4nRR-*tyrd*, though not statistically significant between 4nRR-*tyra* and 4nRR-*tyrd*, were both more highly expressed than that of 4nRR-*tyrb* ($P < 0.05$) (Fig. 3F). In addition, four *tyr* homeologs were both remarkably higher expressed in the 4nRR 12-BY group relative to the 6-BY group ($P < 0.01$) (Fig. 3E). Thus, statistically significant differences in expression were observed among *tyr* homeologs.

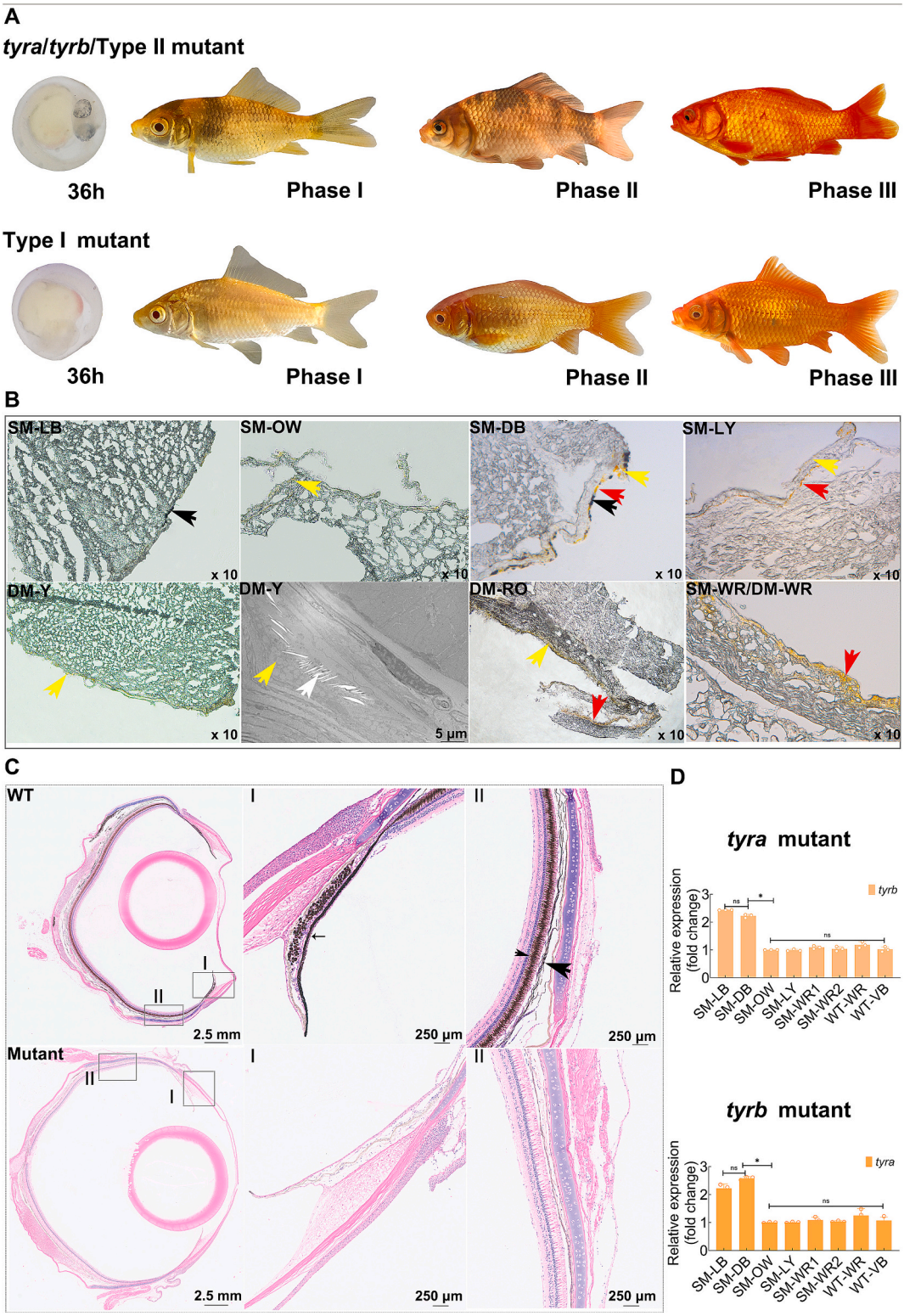

Fig. 4. Two *tyr* homologs synergistically regulate melanogenesis in RCC. A, Pigmentation in four types of *tyr* mutants at different developmental stages. B—C, Pigment cells in the skin (B) and eyes (C) of *tyr* mutant individuals. The red, black, yellow, and white arrows point to erythrophores, melanophores, xanthophores, and iridophores, respectively. Melanin granules in the choroid, retinal pigment epithelia, and iris, are indicated by arrows of different size and ranging from largest to smallest, respectively. D, Expression levels of *tyrb* and *tyra* in the *tyra* and *tyrb* chimeric RCC mutants, respectively (n = 3 individuals). Each point represents the mean of three technical replicates from each individual. Scale bars are shown at the bottom-right corners of the images. Asterisks show statistically significant differences. ns, not significant; *, $P < 0.05$. (For interpretation of the references to color in this figure legend, the reader is referred to the web version of this article.)

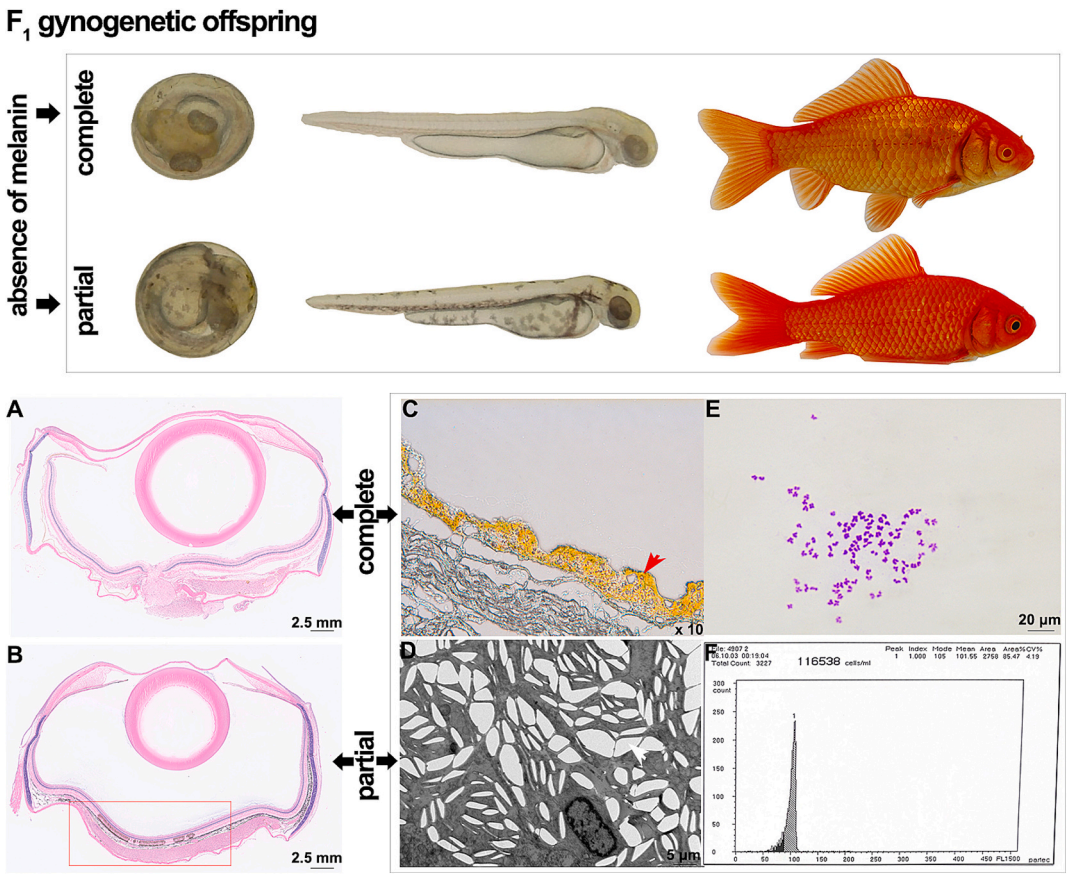

Fig. 5. Establishment, phenotype, chromatophores, and DNA content of F_1 gynogenetic offspring generated from F_0 Type I RCC individuals with complete melanin deficiency. A–B, Pigment cells in the eyes of adult F_1 gynogenetic offspring with complete melanin deficiency (A) and partial melanin loss (B). C—D, Pigment cells in the skin of adult F_1 gynogenetic offspring. The red and white arrows point to erythrophores and iridophores, respectively. E, Chromosome numbers of F_1 gynogenetic offspring. F, The DNA mean content of F_1 gynogenetic offspring. The mean DNA content of F_1 gynogenetic offspring is 101.55. Scale bars are shown at the bottom-right corners of the images. Red box represents partially melanin-deficient region in eyes of adult F_1 gynogenetic offspring. (For interpretation of the references to color in this figure legend, the reader is referred to the web version of this article.)

3.6. Impaired melanin synthesis in tyra or tyrb single-mutated RCC

Comparisons of amino acid identity and expression profiles of *tyra* and *tyrb* in RCC indicated that their functions in melanin synthesis may have diverged. To evaluate this hypothesis, *tyra* and *tyrb* were singly and simultaneously disrupted in RCC. Unexpectedly, both *tyra* chimeric F_0 RCC fish ($n = 50$) and *tyrb* chimeric F_0 RCC fish (n = 50) exhibited similar chimeric phenotypes, characterized by reduced or complete absence of melanin in discrete regions that manifest as patches or stripes (Fig. 4A). Notably, statistically significant differences were not observed in the proportion of skin melanin deposition area between *tyra* ($n = 50$) or *tyrb* mutants (n = 50) ($P > 0.05$), rendering their respective contributions to melanin synthesis inconclusive. Further, genetic analysis of *tyra* chimeric mutants ($tyra^{-4} + tyrb^{+}$) and *tyrb* chimeric mutants ($tyra^{+} + tyrb^{\#5,\ -18,\ -17}$) revealed base deletions, insertions or substitutions, resulting in a shift in reading frame shifts (Supplementary Fig. S6).

Two types of *tyr* single mutant individuals exhibited strikingly similar coloration and pigmentation patterns, with four discrete phenotypic manifestations observed throughout their developmental stages (Fig. 4A). At the initial embryonic stage (36 h after microinjection), partial loss of melanin was noticed in pupils, primarily via melanophores, since they are the pigment cells that are first observed in RCC. As the mutants progressed through developmental stages, increased abundances of melanophores and xanthophores resulted in the appearance of yellowish skin interspersed with black spots or stripes (SM-LB) and eyes with partial melanin (phase I). Subsequently, further increases in melanophores, xanthophores, and erythrophores led to yellow skins (SM-LY) and eyes with partial melanin, embellished with dark-black spots or stripes (SM-DB) (phase II). Finally, decreased abundances of in melanophores and xanthophores coupled with increases in erythrophores led to mutants appearing with red bodies and partially melanin-deficient eyes (SM-WR1 and SM-WR2) (phase III) (Fig. 4B, C).

To further identify the cooperative roles of *tyra* and *tyrb* in RCC, the dynamic expressional changes of *tyrb* were evaluated in *tyra* chimeric mutants ($n = 3$) and *tyra* in *tyrb* chimeric mutants (n = 3) at different developmental stages. Expressional profiles in the *tyrb* in *tyra* mutants were consistent with those of the *tyra* in *tyrb* mutants. Relative to the SM-OW, SM-LY, SM-WR1, SM-WR2, and WT-WR, unspoiled *tyr* showed a dramatic upregulation in expression within SM-LB and SM-DB ($P < 0.05$), but significance differences in expression were not observed between SM-LB and SM-DB ($P > 0.05$) (Fig. 4 D). The expression of unspoiled *tyr* was significantly higher in deep-black and light-black skin than in other samples ($P < 0.05$), similar to *tyr* expression characteristics in wild-type RCC at different developmental stages. Consequently, further analyses of the expression levels of *tyrb* in *tyra* mutants were evaluated in SM-LB, SM-DB and WT-VB, in addition to *tyra* in *tyrb* mutants in SM-LB, SM-DB, and WT-VB. The expression levels of unspoiled *tyr* in both mutants were significantly higher than in wild type ($P < 0.05$) (Fig. 4 D), indicating that unspoiled *tyr* may potentially fill a compensatory role in the melanin synthesis of mutants.

3.7. Absence of melanin in tyra and tyrb double-mutated RCC

Mutants derived from simultaneous disruption of *tyra* and *tyrb* were

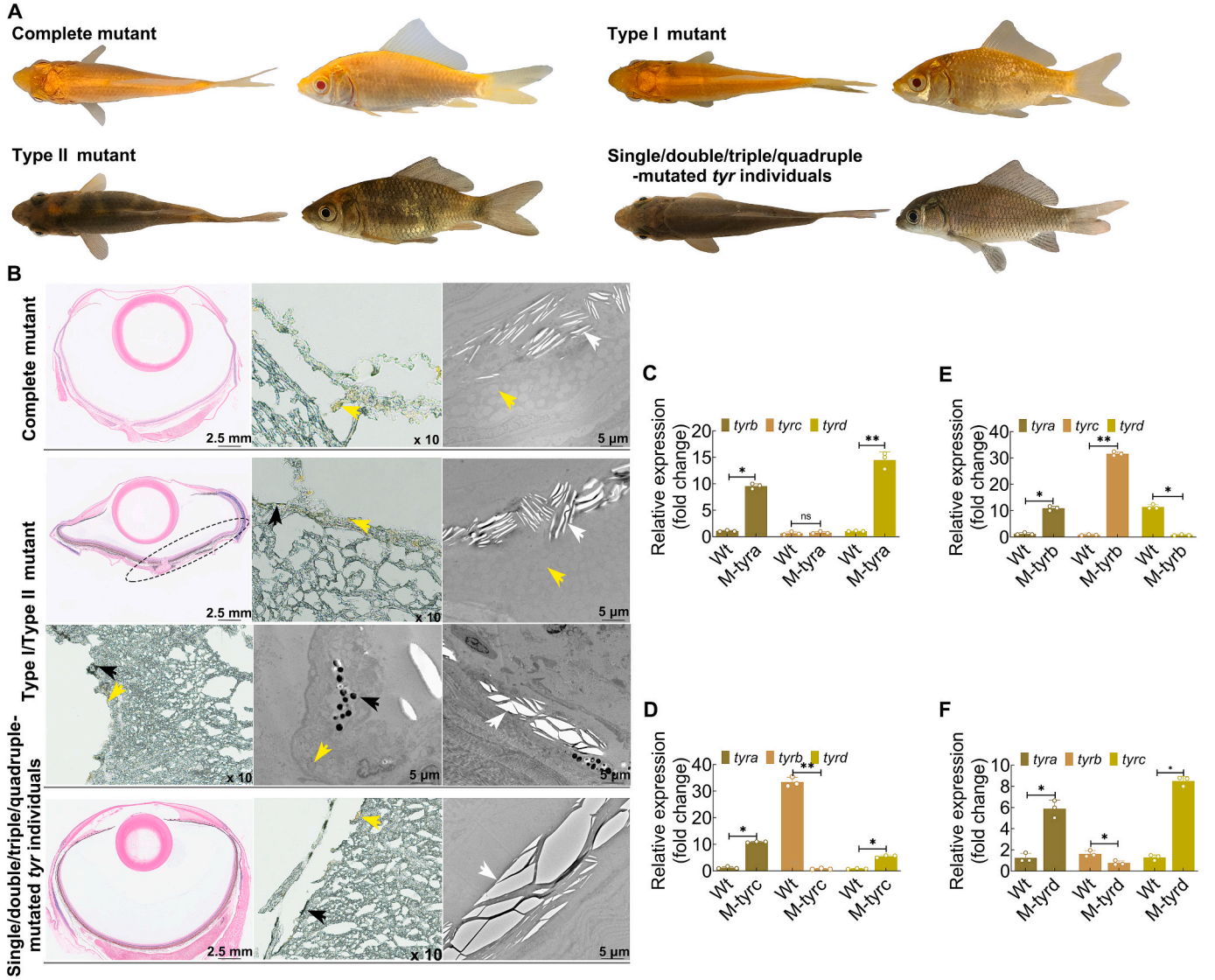

Fig. 6. Generation of the yellowish phenotype in 4nRR. A, Phenotypes of sixteen *tyr* mutant types. B, Identification of pigment cells in different *tyr* mutant individuals. The black, yellow and white arrows indicate melanophore, xanthophores, and iridophores respectively. C—F, Transcriptional expression analyses of three unspoilt *tyr* (C) in the *tyra* chimeric mutant, three unspoilt *tyr* (D) in the *tyrb* chimeric mutant, three unspoilt *tyr* (E) in the *tyrc* chimeric mutant, three unspoilt *tyr* (F) in the *tyrd* chimeric mutant individuals. Scale bars are shown at the bottom-right corners of the images. Statistically significant differences are illustrated by asterisks. ns, not significant; *, $P < 0.05$; **, $P < 0.01$. (For interpretation of the references to color in this figure legend, the reader is referred to the web version of this article.)

classified into Type I mutants ($n = 50$; 90 % of mutants) exhibiting complete melanin deficiency throughout the body, and the remainder as Type II mutants (n = 50) that exhibited coloration phenotypes similar to those observed in *tyra* or *tyrb* single-mutated individuals. Observation of Type I mutants throughout coloration development demonstrated that fish bodies exhibited three different coloration periods, sequentially transitioning from yellowish to orange-yellow, ultimately culminating in red coloration (Fig. 4A). Within the dynamic coloration phases, initial yellowish skin was characterized by the presence of xanthophores and iridophores, alongside increased abundances of erythrophores, marking the transition into the orange-yellow phase that contained containing xanthophores, erythrophores and iridophores. Finally, as xanthophores exhibited gradual decreases until their eventual disappearance, red-like appearances (i.e., red bodies and eyes) resembling the wild-type was observed (Fig. 4B, C). Although the coloration pattern of Type II mutants was similar to that of the single-mutated individuals throughout their development stages, Type II mutants retained a relatively smaller proportion of melanin on the body surfaces during both phases I and II. In addition, analysis of clones indicated the lack of wild-type *tyra* and *tyrb* sequences in Type I individuals, while Type II individuals contained some wild-type sequences (Supplementary Fig. S6).

An F_0 Type I female with complete melanin deficiency was selected for artificial gynogenesis. The diploid offspring were classified into two types according to their melanin content with 97 % of analyzed F_1 gynogenetic offspring ($n = 194$) exhibiting an absolute absence of melanin, and the rest of the F_1 gynogenetic offspring ($n = 6$) characterized by black spots or stripes that were morphologically similar to F_0 Type II individuals (Fig. 5). Six individuals from two groups of F_1 gynogenetic offspring were respectively sampled to investigate their genotypes. One mutated genotype from the F_1 gynogenetic offspring with an absolute absence of melanin was detected, in which both the *tyr* homeologs were mutated into a premature stop codon (Supplementary Fig. S7). The individuals in a different group comprised two mutated genotypes wherein all mutants possessed mutated and wild-type *tyr* sequences (Supplementary Fig. S7). Notably, a homozygous mutant individual ($tyra^{-4} + tyrb^{-4}$) was generated through artificial gynogenesis.

In summary, these results suggest that the complete disruption of both *tyra* and *tyrb* can inhibit melanin synthesis, resulting in absolute

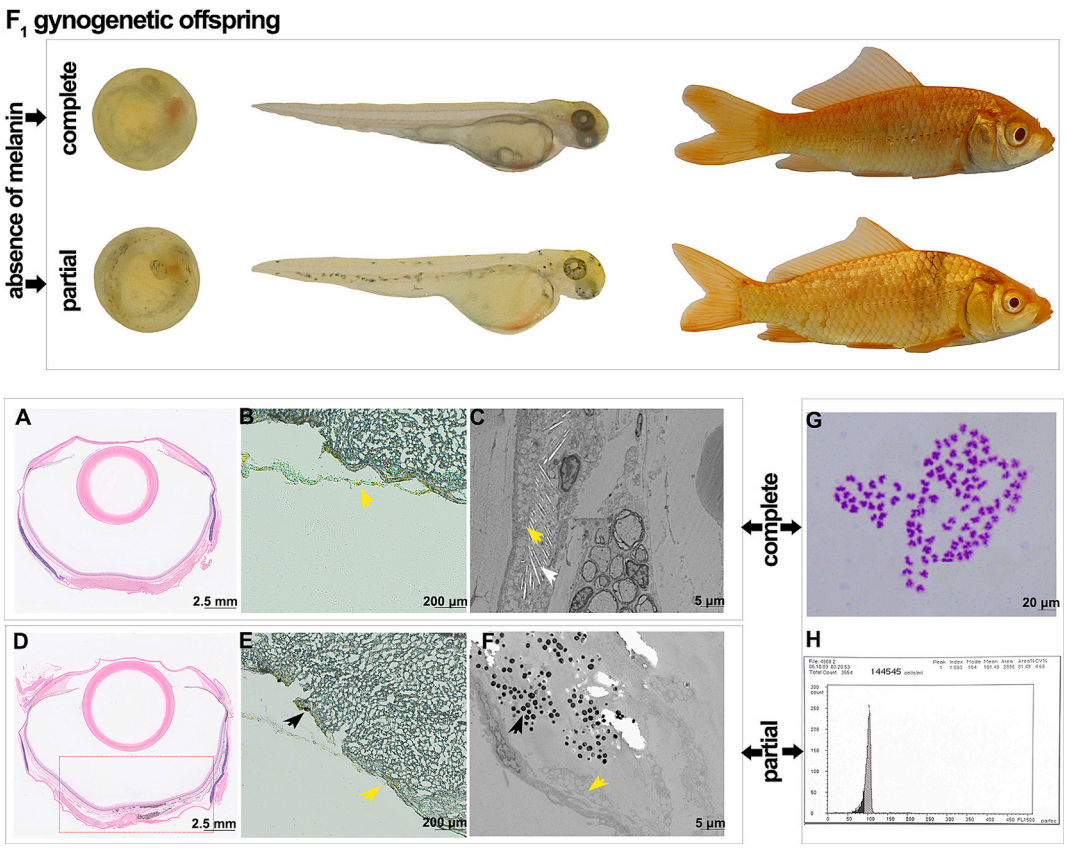

Fig. 7. Establishment, phenotype, chromatophores, and DNA content of diploid F_1 gynogenetic offspring generated from 4nRR individuals with complete melanin defects. A–C, Pigment cells in the eyes (A) and skins (B, C) of adult F_1 gynogenetic offspring with complete melanin deficiency. D—F, Pigment cells in the eyes (A) and skins (B, C) of adult F_1 gynogenetic offspring with partial melanin loss. The black, yellow, and white arrows point to melanophores, xanthophores, and iridophores, respectively. G, Chromosome numbers of F_1 diploid gynogenetic offspring. H, The DNA mean content of diploid F_1 gynogenetic offspring. The mean DNA content of F_1 gynogenetic offspring is 101.48. Scale bars are shown at the bottom-right corners of the images. Red box represents partially melanin-deficient region in eyes of diploid F_1 gynogenetic offspring. (For interpretation of the references to color in this figure legend, the reader is referred to the web version of this article.)

loss of melanin throughout the body, while partial melanin loss can be caused by the functional deficiency of a single *tyr* gene. Combined with the significantly higher expression of the unspoiled *tyr* in *tyr* single-mutated RCC compared to wild-type, the results described above indicate that two *tyr* homologs are required for coloration in RCC, but have sub-functionalized to synergistically regulate melanogenesis in RCC.

3.8. Simultaneous deficiency of four tyr homeologs is required for the yellowish phenotype in 4nRR

As described above, the *tyra* homeologs of 4nRR fish completely originated from RCC-*tyra*, while the other three *tyr* homeologs originated via a duplication from RCC-*tyr*. Divergent expression patterns of these homeologs were observed, implying potential functional and evolutionary divergence following auto-tetraploidization. To explore the functional roles and related processes for the four *tyr* homeologs in coloration formation and pigmentation variation in 4nRR, the morphologies and the histological structures of skins and eyes were compared among single-mutated, multiple-mutated (<4), and simultaneously-mutated *tyr* mutants. Four types of *tyr* single-mutated 4nRR mutants, including *tyra* mutants ($tyra^{\#4,\ -11} + tyrb^{+} + tyrc^{+} + tyrd^{+}$) ($n = 20$), *tyrb* mutants ($tyra^{+} + tyrb^{-2,\ +6} + tyrc^{+} + tyrd^{+}$) (n = 20), *tyrc* mutants ($tyra^{+} + tyrb^{+} + tyrc^{-5,\ -2,\ +16} + tyrd^{+}$) (n = 20), and *tyrd* mutants ($tyra^{+} + tyrb^{+} + tyrc^{+} + tyrd^{-9,\ -9,\ -26,\ -9}$) (n = 20), exhibited unaltered phenotypes and pigment cell compositions, resembling wild-type-like individuals (Fig. 6A, B, Supplementary Fig. S8), inconsistent with the expectations of impaired melanogenesis observed in *tyra* or *tyrb* single-mutated RCC mutants. Furthermore, specific sgRNAs demonstrated notable efficiency in simultaneously targeting multiple *tyr* homeologs (<4) due to the extremely high genetic identity among the four *tyr* homeologs. These dynamics resulted in the generation of *tyra-tyrb*-mutated ($tyra^{-9} + tyrb^{-1} + tyrc^{+} + tyrd^{+}$), *tyra-tyrc*-mutated ($tyra^{-18} + tyrb^{+} + tyrc^{-35/-35} + tyrd^{+}$), *tyra-tyrd*-mutated ($tyra^{-20} + tyrb^{+} + tyrc^{+} + tyrd^{-7,\ \#4,\ \#2,\ +3}$), *tyrb-tyrc*-mutated ($tyra^{+} + tyrb^{+3} + tyrc^{-35/-23} + tyrd^{+}$), *tyrb-tyrd*-mutated ($tyra^{+} + tyrb^{-3,\ +6} + tyrc^{+} + tyrd^{-11/-11}$), *tyrc-tyrd*-mutated ($tyra^{+} + tyrb^{+} + tyrc^{\#3,\ -11/-10/-44} + tyrd^{-9,\ -9}$), *tyra-tyrb-tyrc*-mutated ($tyra^{\#2,\ -9,\ +5} + tyrb^{-2,\ +14} + tyrc^{-5,\ -6,\ \#2,\ -2/-5,\ -3,\ \#1,\ -5,\ \#1} + tyrd^{+}$), *tyra-tyrb-tyrd*-mutated ($tyra^{\#4/\#4,\ -9} + tyrb^{-2} + tyrc^{+} + tyrd^{-4,\ +3/-11,\ -12,\ +13}$), *tyrb-tyrc-tyrd*-mutated ($tyra^{+} + tyrb^{-4} + tyrc^{-6/\#2,\ -1,\ +16} + tyrd^{-8,\ -10/\#2,\ -8,\ -10}$), and *tyra-tyrc-tyrd*-mutated ($tyra^{\#4/-11} + tyrb^{+} + tyrc^{-26} + tyrd^{-9,\ -9/-26,\ -9}$) 4nRR mutants. Interestingly, coloration phenotype and chromatophores in all *tyr* multiple-mutated individuals were unaffected, resulting in brownish-yellow phenotypes (Fig. 6A, B, Supplementary Fig. 8).

Simultaneous deficiency of four *tyr* homeologs was required to achieve reduced or absent melanin in 4nRR individuals. Mutants were classified into complete mutants exhibiting systemic melanin loss that exhibited yellowish coloration with only xanthophores and iridophores in skins and the absence of melanin in eyes or alternatively, chimeric mutants retaining partial melanin characteristics that resulted in the emergence of black spots or stripes with xanthophores and melanophores, alongside yellowish areas (Fig. 6B) containing xanthophores and iridophores. Approximately 10 % of chimeric individuals classified as Type I mutants ($n = 50$), had a ratio of melanin to yellowish area < 0.5, while Type II mutants (n = 50) exhibited ratios >0.5. Blood DNA extraction, amplification of effective target regions and cloning of the

three aforementioned mutants were conducted. The proportion of wild-type sequences of these three *tyr* homeologs included (in descending order): Type II chimeric mutants, Type I chimeric mutants, and complete mutants. The corresponding monoclonal results of mutation types are shown in Supplementary Fig. S9. The expression patterns of undisrupted *tyr* in four types of *tyr* single-mutated mutant skins were significantly higher than in wild-type individuals (Fig. 6C–F).

To identify the roles and associations of the four *tyr* homeologs to skin color changes in 4nRR individuals, three 4nRR individuals with complete melanin defects were chosen for proliferation by gynogenesis. This resulted in diploid offspring with half sets of 4nRR-derived chromosomes, enabling detailed investigation of phenotypes and genotypes of F_1 offspring in these gynogenetic mutants. The diploid F_1 gynogenetic offspring were morphologically similar to complete mutants or Type I chimeric mutants. The offspring were classified into two types according to melanin patterns: those with yellowish bodies and yellowish eyes ($n = 308$), and those with yellowish bodies or eyes with black spots or stripes (n = 30) (Fig. 7). In particular, one gynogenetic clone (mutant-1) exhibited stark differences relative to the other two gynogenetic clones ($n = 78/98$, 79.6 % yellowish mutant-2; $n = 80/92$, 86.9 % yellowish mutant-3), with about 94.1 % of offspring ($n = 111/118$) exhibiting yellowish coloration and 5.9 % of offspring (n = 7/118) exhibiting varying degrees of melanin defects. Consequently, the chromatophores of five individuals from complete gynogenetic F_1 offspring and another group with various degrees of melanin defects were respectively identified. The mutated genotypes of these offspring were evaluated with PCR amplification and subsequent clonal sequencing. Xanthophores and iridophores were observed in the skin of the former group, while xanthophores, iridophores, and melanophores were identified in the latter group (Fig. 7). All five of the yellowish gynogenetic offspring possessed the different mutated genotypes (Supplementary Fig. S10), wherein the mutation of four *tyr* generated a premature stop codon. Different genotypes of the five individuals were also identified that possessed some WT sequences of *tyr* (Supplementary Fig. S11).

The above data indicated that melanin synthesis was unaffected in *tyr* single−/double−/triple-mutated 4nRR individuals. However, reduced or absent melanin was only achieved when all *tyr* were simultaneously dysfunctional. Consequently, melanin synthesis in 4nRR may be normally maintained when least one functional *tyr* homeolog is present. Overall, these results suggest that all *tyr* have evolved to cooperatively regulate 4nRR melanogenesis following autopolyploidization.

4. Discussion

Trait and genetic variation induced by polyploidization has long-been a topic of interest for evolutionary biology and genetics (Gui et al., 2022; Song et al., 2012; Zhou and Gui, 2017). Investigations of genome variation and evolution in polyploid animals have provided some important insights. The genome of autotetraploid *Carassius auratus* originated from the WGD of RCC and exhibits genomic and epigenetic alterations, rendering it an excellent model to comprehensively evaluate the evolutionary fate and functional divergence of genes after WGD. Here, the genetic variation and functional regulation of differentially expressed *tyr* genes in coloration formation and change following autopolyploidization were investigated in comparisons of red RCC and brownish-yellow 4nRR fish. Specifically, differences in chromatophores, melanin, and skin transcriptomic profiles were used to assess overall physiological restructuring. The *tyr* homeologs were shown to sub-functionalized to synergistically and non-differentially govern melanogenesis in RCC. However, in 4nRR, all *tyr* homeologs were shown to have evolved into dominant roles in melanogenesis, resulting in cooperative involvement in 4nRR coloration formation and change, that was entirely different from regulatory characteristics in RCC. Following autopolyploidization, four *scarb1* homeologs were sub-functionalized and are now required for 4nRR pigmentation, with all *scarb1* genes synergistically and equally contributing to 4nRR pigmentation (Xu et al., 2024). These results indicate that the regulation of color formation and variation in 4nRR is highly complicated.

The diversity of coloration and pigment patterns in fish species are generated by the combined distributions of various pigment cells, coupled with distributions in the types, proportions, and densities of intracellular pigments, with melanophores and melanin being the most comprehensively evaluated (Lin and Fisher, 2007). In this study, the melanin contents of red RCC without melanophores were extremely significantly lower than in 4nRR that possessed melanophores (Fig. 1G). These results are consistent with previous studies of the loaches *Misgurnus anguillicaudatus* (Sheng et al., 2021), *Plectropomus leopardus* (Deng et al., 2020), *Triplophysa stenura*, and *Triplophysa orientalis* (Zhu et al., 2022). Thus, greater melanin content in tissues with melanophores can generally be observed relative to those with the absence or insufficiency of melanophores. In addition to the widely known *α-MSH* pathway of melanin synthesis, several other pathways (*WNT*, *P13K/AKT*, and *MAPK*) are involved in this process (D'Mello et al., 2016). Interestingly, the "MAPK signaling pathway" was second most enriched in this study and has been reported to be involved in the "melanogenesis pathway" (Lemmon and Schlessinger, 2010). Up-regulated genes of the MAPK signaling pathway further affect the significant up-regulation of *mitf*, *tyr*, and *tyrp1* genes in the melanogenesis pathway of 4nRR. Among these pathways, *tyr* is considered a pivotal regulator that can be directly responsible for regulating eumelanin or pheomelanin pigment synthesis (Solano, 2018). Based on the observed differences in melanin content, transcriptomic profiles, and expression levels of genes related to melanogenesis between the two fishes (Fig. 2D), the *tyr* gene family was further scrutinized for its role in coloration and variation following autotetraploidization.

Carassius auratus red var. is an amphidiploid that is known to have experienced an allotetraploidy event (Luo et al., 2020). In this study, two *tyr* homeologs with high identity were identified in its genome and belonged to two independent phylogenetic groups (Fig. 3A, C), indicating that *tyr* may have been duplicated in the ancestor of RCC (4R). Differences in genetic composition were observed among four divergent *tyr* homeologs that were likely to have originated after autotetraploidization. Similar genetic features showing differences between original genes derived from RCC and duplicated genes have also been noted in *dmc1*, *sox9a*, *amh*, *cyp19a1*, and *scarb1* of 4nRR (Xu et al., 2023; Huang et al., 2020). Previous studies have suggested that these genetic changes may represent a rapid response of the genome to synthetic 4nRR. Furthermore, amino acid variants were notably identified in duplicated 4nRR-*tyrc* and 4nRR-*tyrd* homeologs that respectively originated from the fusion and recombination of RCC-*tyrb* and BSB-*tyr*; RCC-*tyra* and BSB-*tyr* (Fig. 3A), suggesting a hybrid origin of *tyr* paralogues in 4nRR. Similar parental-derived sequence variation and homologous recombination events have also been demonstrated in newly formed allopolyploid fishes and other newly synthesized polyploid plants (Ren et al., 2022; Qin et al., 2019a; Martelotto et al., 2007; Mecchia et al., 2006). These changes result in divergence and increased heterozygosity among homologous genes that can then contribute to enhancing the balance and genetic stability among *tyr* homeologs. Hybridization and polyploidization can link trans-acting factors of different origins to cis-acting elements in promoter regions, thereby altering regulation of gene expression in polyploid genomes (Zhu and Xiao, 2004). Consequently, gene expression tends to be considerably altered after polyploidization, which may be beneficial for polyploid formation, and especially the stability of genomes and rapid adaptations to environmental change (Pikaard, 2001). We recently demonstrated that overall expression differences were present among homeologous genes of A and A' homeologous genomes in 4nRR. Further, a shift in the expression dominance of homeologous genes of two homeologous genomes was observed during embryonic development (unpublished data). In this study, biased expression among *tyr* homeologs was also observed (Fig. 3C–F), which can be seen in previous studies of 4nRR genes (Xu et al., 2023; Huang

et al., 2020). These observations collectively indicate that genetic change and expressional alterations of *tyr* have occurred in 4nRR, suggesting that their genetic composition and expressional characteristics were influenced by autotetraploidization.

Consistent with oculocutaneous albinism type I (OCA1) in human (*Homo sapiens*) (Oetting et al., 1998), *tyr* mutants of numerous animals including mice (*Mus musculus*) (Wang et al., 2013), medaka (*Oryzias latipes*) (Koga et al., 1995), zebrafish (Ota et al., 2014), loach (*Paramisgurnus dabryanus*) (Xu et al., 2019a), rainbow trout (Boonanuntanasarn et al., 2004), yellow catfish (*Tachysurus fulvidraco*) (Zhang et al., 2018), fathead minnow (*Pimephales promelas*) (Maki et al., 2020), anemonefish (*Amphiprion ocellaris*) (Mitchell et al., 2021), Atlantic Salmon (*Salmo salar*) (Edvardsen et al., 2014), white crucian carp (*Carassius auratus cuvieri*) (Liu et al., 2019), and *Xenopus tropicalis* (Blitz et al., 2013) all display hypopigmentation of skin and retinal pigment epithelia. Thus, a conserved role of *tyr* is likely exerted upon melanophore differentiation and melanin synthesis. In this study of RCC, disruption of *tyra* or *tyrb* function resulted in reduced or lost melanin in partial region, while disruption of two *tyr* homeologs caused greater reduction or complete absence of melanin across entire bodies (Fig. 4). The efficient compensatory expression of undisrupted *tyr* in single-mutated RCC in conjunction with phenotypes and genotypes of F_1 gynogenetic offspring suggest that *tyra* and *tyrb* have sub-functionalized following allotetraploidization to synergistically and non-differentially regulate melanogenesis in RCC. Interestingly, specific pigment cells other than melanophores successively appeared or disappeared at corresponding coloration periods throughout coloration development of the mutant individuals, Thus, the absence of melanophores did not seem to affect the appearance of other pigment cells. Furthermore, genes associated with carotenoid metabolism exhibited similar gene expression patterns in both wild-type RCC (GC, OY, and RC) and mutant RCC (DM-Y, DM-OY, and DM-WR), with appropriate and explainable up- and down-regulation, indicating that functional deficiency of *tyr* did not result in altered expression levels of genes involved in xanthophore/erythrophore formation (Supplementary Fig. S12). During pigment cell development in fish, specific neural crest cells derive clusters of embryonic cells via the dorsolateral neural tube that subsequently migrate ventrally to specific locations and eventually differentiate into various types of chromatophores (Hall, 1999). Additionally, some studies have suggested that pigment cells can derive from neural crest cells and also from stem cells (Tu and Johnson, 2010; Mcmenamin et al., 2014). As discussed above, xanthophores/erythrophores in RCC were thought to have solely originated from the differentiation and development of neural crest cells, implying that they may not be associated with melanophores. Considerable more research is needed in this area, including via single cell RNA-seq assays to explore differentiated trajectories during pigment cell development to confirm the possible origin of pigment cells in RCC fish.

After autotetraploidization, the evolutionary fate of *tyr* is another scenario. The results here indicate that *tyr* have evolved to cooperatively regulate 4nRR melanogenesis, that is absolutely different from the regulatory patterns observed in RCC. The genomes of autotetraploid *Carassius auratus* (4nRR, 4n = 200, RRRR) (In NCBI under the accession PRJNA1138278, unpublished) were recently generated, demonstrating that 4nRR originated from the WGD of *Carassius auratus* red var. (RCC, 2n = 100, RR). Furthermore, the sub-functionalization of duplicated *scarb1* homeologs following autotetraploidization was also further investigated. The phenotypes of the four *tyr* single-mutated and ten types of *tyr* multiple-mutated (<4) 4nRR were all exactly identical, with none of them differing from the pigmentation and pigmented cell characteristics observed in wild-type individuals (Fig. 6). These results are inconsistent with biased expression among *tyr* homeologs. In contrast, the simultaneous disruption of four *tyr* homeologs resulted in reduced or absent melanogenesis, generating a chimeric or albino phenotype (Fig. 6). The roles of *tyr* in the melanin synthesis of both fishes are extremely conserved, but all *tyr* homeologs appear to have evolved to have dominant roles in melanogenesis in 4nRR relative to the sub-functionalization of both *tyr* homeologs in RCC, suggesting that genetic change and evolutionary regulation of *tyr* was drastically influenced by autotetraploidization. 4nRR possess four different *tyr* homeologs and it thus considerably more difficult to establish homozygous mutant 4nRR strains compared to diploid RCC. Mutated 4nRR females were able to produce autodiploid eggs (2n = 100) after activation by UV-irradiated BSB sperm, with the autodiploid eggs developing into mutated all-female autodiploid gynogenetic offspring without chromosome doubling treatment. Moreover, autodiploid gynogenetic offspring have been shown to reproduce by gynogenesis when their unreduced diploid eggs were fertilized by sperm from BSB (Qin et al., 2018). Thus, the melanin-deficient mutated autodiploid gynogenetic offspring can be easily used to further create melanin-free autodiploid gynogenetic offspring strains via successive generations of gynogenesis in order to generate polyploid fish with novel coloration patterns by crossing with other fishes.

5. Conclusion

In conclusion, chromatophore and melanin differences were observed between RCC and 4nRR in this study, while key genes involved in melanin-based coloration were investigated, revealing effective and differential regulation of *tyr* in the formation and variation of pigmentation in 4nRR due to autotetraploidization. The results of this study provide new insights into the molecular mechanisms underlying pigmentation and coloration variations in 4nRR, but also provide an important resource to inform skin color–based genetic breeding in polyploid fishes.

Compliance and ethics

The authors declare that they have no conflict of interest.

Author contribution

Qin-Bo Qin designed the study and Shao-Jun Liu provided expert comments. Xi-Dan Xu provided the preliminary data that supported this study. Yue Zhou, Jin-Hai Bai, Xu Huang, Zheng-Kun Liu, Xin-Yi Deng, Yan Tang, Wan-Jing Peng, Ling Xiong, and Ming Ma performed the daily animal care. Chong-Qing Wang, Kun Zhang and Xiao-Wei Xu performed the analyses of the other data. Xi-Dan Xu wrote the manuscript. All authors read and approved the final manuscript.

CRediT authorship contribution statement

Wan-Jing Peng: Methodology. **Yue Zhou:** Methodology. **Chong-Qing Wang:** Methodology. **Kun Zhang:** Methodology. **Xu Huang:** Methodology. **Xiao-Wei Xu:** Methodology. **Jin-Hai Bai:** Methodology. **Ling Xiong:** Methodology. **Zheng-Kun Liu:** Methodology. **Xin-Yi Deng:** Methodology. **Yan Tang:** Methodology. **Ming Ma:** Methodology. **Shao-Jun Liu:** Conceptualization, Writing – review & editing. **Xidan Xu:** Writing – original draft. **Qinbo Qin:** Writing – review & editing.

Declaration of competing interest

The authors declare that they have no conflict of interest.

Data availability

Raw RNA-Seq reads are available from the NCBI (PRJNA932244). The obtained tyr gene sequences are available from the NCBI (RCC-tyra GeneBank: OP466737; RCC-tyrb GeneBank: OP466738; 4nRR-tyra GeneBank: OP466739; 4nRR-tyrb GeneBank: OP466740; 4nRR-tyrc GeneBank: OP466741; 4nRR-tyrd GeneBank: OP466742). Supplementary Table S3 (DOI: 10.6084/m9.figshare.26892172; https://figshare.com/articles/dataset/Differentially_expressed_genes_DEGs_in_i_Carassius_auratus_i_red_var_vs_autotetraploid_i_Carassius_auratus_i_/26892172?file=48930133). Supplementary Table S4 (DOI: 10.6084/m9.figshare.26891635; https://figshare.com/articles/dataset/DEGs_involved_in_the_biological_process_category_based_on_gene_ontology_GO_enrichment_analysis_of_i_Carassius_auratus_i_red_var_and_b_autotetraploid_b_b_i_Carassius_auratus_i_b_skin_/26891635?file=48929080). Supplementary Table S5 (DOI: 10.6084/m9.figshare.26892235; https://figshare.com/articles/dataset/DEGs_involved_in_the_b_b_cellular_component_category_based_on_gene_ontology_GO_enrichment_analysis_of_i_Carassius_auratus_i_red_var_and_autotetraploid_i_Carassius_auratus_i_fish_/26892235?file=48930253). Supplementary Table S6 (DOI: 10.6084/m9.figshare.26892307; https://figshare.com/articles/dataset/DEGs_involved_in_the_b_b_molecular_function_category_based_on_gene_ontology_GO_enrichment_analysis_of_i_Carassius_auratus_i_red_var_and_autotetraploid_i_Carassius_auratus_i_fish_/26892307?file=48930313).

Acknowledgements

This work was financially supported by the National Natural Science Foundation of China (Grant No. 32172972), the Science and Technology Innovation Program of Hunan Province (Grant No. 2021RC4028), and the Special Funds for Construction of Innovative Provinces in Hunan Province (Grant No. 2021NK1010), Special Science Found of Nansha-South China Agricultural University Fishery Research Institute, Guangzhou (NSYYKY202305 and NSYYKY202306), the Aid Program for Science and Technology Innovative Research Team in Higher Educational Institutions of Hunan Province, the earmarked fund for HARS (HARS-07). We thank LetPub (www.letpub.com.cn) for linguistic assistance.

Appendix A. Supplementary data

Supplementary data to this article can be found online at https://doi.org/10.1016/j.aquaculture.2024.741952.

References

Abràmoff, M.D., Magalhães, P., Ram, S.J., 2004. Image processing with ImageJ. Biophoton. Int. 11, 36–42.
Amores, A., Force, A., Yan, Y.L., Joly, L., Amemiya, C., Fritz, A., Ho, R.K., Langeland, J., Prince, V., Wang, Y.L., Westerfield, M., Ekker, M., Postlethwait, J.H., 1998. Zebrafish hox clusters and vertebrate genome evolution. Science 282 (5394), 1711–1714.
Anders, S., Huber, W., 2010. Differential expression analysis for sequence count data. Genome Biol. 11, R106.
Awan, M.J.A., Rasheed, A., Saeed, N.A., Mansoor, S., 2022. *Aegilops tauschii* presents a genetic roadmap for hexaploid wheat improvement. Trends Genet. 38 (4), 307–309.
Berthelot, C., Brunet, F., Chalopin, D., Juanchich, A., BernardM Noel, B., Bento, P., Silva, C.D., Labadie, K., Alberti, A., Aury, J.M., Louis, A., Dehais, P., Bardou, P., Montfort, J., Klopp, C., Cabau, C., Gaspin, C., Thorgaard, G.H., Boussaha, M., Quillet, E., Guyomard, R., Galiana, D., Bobe, J., Volff, J.N., Genêt, C., Wincker, P., Jaillon, O., Crollius, H.R., Guiguen, Y., 2014. The rainbow trout genome provides novel insights into evolution after whole-genome duplication in vertebrates. Nat. Commun. 5 (1), 3657.
Blitz, I.L., Biesinger, J., Xie, X., Cho, K.W., 2013. Biallelic genome modification in F0 *Xenopus tropicalis* embryos using the CRISPR/Cas system. Genesis 51 (12), 827–834.
Boonanuntanasarn, S., Yoshizaki, G., Iwai, K., Takeuchi, T., 2004. Molecular cloning, gene expression in albino mutants and gene knockdown studies of tyrosinase mRNA in rainbow trout. Pigm. Cell Melanoma Res. 17 (4), 413–421.
Braasch, I., Schartl, M., Volff, J.N., 2007. Evolution of pigment synthesis pathways by gene and genome duplication in fish. BMC Evol. Biol. 7 (1), 74.
Braasch, I., Brunet, F., Volff, J.N., Schartl, M., 2009. Pigmentation pathway evolution after whole-genome duplication in fish. Genome Biol. Evol. 1, 479–493.
Chen, Z.J., Sreedasyam, A., Ando, A., Song, Q.X., Santiago, L.M.D., Hulse-Kemp, A.M., Ding, M.Q., Ye, W.X., Kirkbride, R.C., Jenkins, J., Plott, C., John Lovell, J., Lin, Y.M., Vaughn, R., Liu, B., Simpson, S., Scheffler, B.E., Wen, L., Saski, C.A., Grover, C.E., Hu, G.J., Conover, J.L., Carlson, J.W., Shu, S.Q., Boston, L.B., Williams, M., Peterson, D.G., McGee, K., Jones, D.C., Wendel, Jonathan F., J.F., Stelly, D.M., Grimwood, J., Schmutz, J., 2020. Genomic diversifications of five *Gossypium* allopolyploid species and their impact on cotton improvement. Nat. Genet. 52 (5), 525–533.
Corneillie, S., De Storme, N., Van Acker, R., Fangel, J.U., Michiel De Bruyne, M.D., Rycke, R.D., Geelen, D., Willats, W.G.T., Vanholme, B., Wout Boerjan, W., 2019. Polyploidy affects plant growth and alters cell wall composition. Plant Physiol. 179 (1), 74–87.
Deng, C., Chen, S.L., Ye, H.Z., Qi, X.Z., Luo, J., 2020. Analysis of pigment and enzyme levels of *Plectropomus leopardus* with body color difference. Life Sci. Res. 24 (1), 15–20.
D'Mello, S.A., Finlay, G.J., Baguley, B.C., Askarian-Amiri, M.E., 2016. Signaling pathways in melanogenesis. Int. J. Mol. Sci. 17 (7), 1144.
Edvardsen, R.B., Leininger, S., Kleppe, L., Skaftnesmo, K.O., Wargelius, A., 2014. Targeted mutagenesis in Atlantic salmon (*Salmo salar* L.) using the CRISPR/Cas9 system induces complete knockout individuals in the F0 generation. PLoS One 9 (9), e108622.
Gotz, S., Garcia-Gomez, J.M., Terol, J., Williams, T.D., Nagaraj, S.H., Nueda, M.J., Robles, M., Talón, M., Dopazo, J.Q., Conesa1, A., 2008. High-throughput functional annotation and data mining with the Blast2GO suite. Nucleic Acids Res. 36 (10), 3420–3435.
Gui, J.F., Zhou, L., Li, X.Y., 2022. Rethinking fish biology and biotechnologies in the challenge era for burgeoning genome resources and strengthening food security. Water Biol. Sec. 1 (1), 100002.
Hall, B.K., 1999. The Neural Crest in Development and Evolution. Springer, New York, NY.
Hu, F.Z., Zhong, H.T., Fan, J.J., Wu, C., Wang, S., Wang, Y.D., Luo, K.K., Zhao, R.R., Liu, J.H., Qin, Q.Q., Tang, C.C., Liu, S.J., 2020. A new type of tetraploid fish derived via female autotetraploid × male allotetraploid hybridization. Aquaculture 524, 735244.
Huang, X., Qin, Q.B., Gong, K.J., Wu, C., Zhou, Y.W., Chen, Q., Feng, W.J., Xing, Y.Y., Wang, C.Q., Wang, Y.D., Cao, L., Tao, M., Liu, S.J., 2020. Comparative analyses of the *Sox9a-Amh-Cyp19a1a* regulatory cascade in autotetraploid fish and its diploid parent. BMC Genet. 21 (1), 35.
Kassahn, K.S., Dang, V.T., Wilkins, S.J., Perkins, A.C., Ragan, M.A., 2009. Evolution of gene function and regulatory control after whole-genome duplication: comparative analyses in vertebrates. Genome Res. 19 (8), 1404–1418.
Koga, A., Inagaki, H., Bessho, Y., Hori, H., 1995. Insertion of a novel transposable element in the tyrosinase gene is responsible for an albino mutation in the medaka fish, *Oryzias latipes*. Mol. Gen. Genet. 249 (4), 400–405.
Kumar, S., Stecher, G., Tamura, K., 2016. MEGA7: Molecular evolutionary genetics analysis version 7.0 for bigger datasets. Mol. Biol. Evol 33 (7), 1870–1874.
Lemmon, M.A., Schlessinger, J., 2010. Cell signaling by receptor tyrosine kinases. Cell 141 (7), 1117–1134.
Li, H., Handsaker, B., Wysoker, A., 2009. The sequence alignment/map format and SAMtools. Bioinformatics 25 (16), 2078–2079.
Lin, J.Y., Fisher, D.E., 2007. Melanocyte biology and skin pigmentation. Nature 445 (7130), 843–850.
Liu, S., Luo, J., Chai, J., Ren, L., Zhou, Y., Huang, F., Liu, X., Chen, Y., Zhang, C., Tao, M., Liu, B., Zhou, W., Lin, G.L., Mai, C., Yuan, S., Wang, J., Li, T., Qin, Q.B., Fang, H., Luo, K.K., Xiao, J., Zhong, H., Zhao, R.R., Duan, W., Song, Z.Y., Wang, Y.Q., Wang, J., Zhong, L., Wang, L., Ding, Z.L., Du, Z.L., Lu, X.M., Gao, Y., Murphy, R.W., Liu, Y., Meyer, A., Zhang, Y.P., 2016. Genomic incompatibilities in the diploid and tetraploid offspring of the goldfish x common carp cross. Proc. Natl. Acad. Sci. USA 113 (5), 1327–1332.
Liu, Q.F., Qi, Y.H., Liang, Q.L., Song, J., Liu, J.M., Li, W.H., Shu, Y.Q., Tao, M., Zhang, C., Qin, Q.B., Wang, J., Liu, S.J., 2019. Targeted disruption of tyrosinase causes melanin reduction in *Carassius auratus cuvieri* and its hybrid progeny. Sci. China Life Sci. 62 (9), 1194–1202.
Livak, K.J., Schmittgen, T.D., 2001. Analysis of relative gene expression data using real-time quantitative PCR and the 2(-Delta Delta C(T)) method. Methods (San Diego, Calif.) 25 (4), 402–408.
Luo, J., Gao, Y., Ma, W., Bi, X.Y., Wang, S.Y., Wang, J., Wang, Y.Q., Chai, J., Du, R., Wu, S.F., Meyer, A., Zan, R.G., Xiao, H., Murphy, R.W., Zhang, Y.P., 2014. Tempo and mode of recurrent polyploidization in the *Carassius auratus* species complex (Cypriniformes, Cyprinidae). Heredity 112 (4), 415–427.
Luo, J., Chai, J., Wen, Y., Tao, M., Zhang, Y.P., 2020. From asymmetrical to balanced genomic diversification during rediploidization: subgenomic evolution in allotetraploid fish. Sci. Adv. 6 (22) eaaz7677.
Ma, W., Zhu, Z.H., Bi, X.Y., Murphy, R.W., Wang, S.Y., Gao, Y., Xiao, H., Zhang, Y.P., Luo, J., 2014. Allopolyploidization is not so simple: evidence from the origin of the tribe cyprinini (Teleostei: Cypriniformes). Curr. Mol. Med. 14 (10), 1331–1338.
Maki, J.A., Cavallin, J.E., Lott, K.G., Saari, T.W., Ankley, G.T., Villeneuve, D.L., 2020. A method for CRISPR/Cas9 mutation of genes in fathead minnow (*Pimephales promelas*). Aquat. Toxicol. 222, 105464.
Martelotto, L.G., Ortiz, J.P.A., Stein, J., Espinoza, F., Quarin, C.L., Pessino, S.C., 2007. Genome rearrangements derived from autopolyploidization in *Paspalum* sp. Plant Sci. 172 (5), 970–977.
McClintock, B., 1984. The significance of responses of the genome to challenge. Science 226 (4676), 792–801.
Mcmenamin, S.K., Bain, E.J., Mccann, A.E., Patterson, L.B., Eom, D.S., Waller, Z., Hamill, J.C., Kuhlman, J.A., Eisen, J.S., Parichy, D.M., 2014. Thyroid

hormone–dependent adult pigment cell lineage and pattern in zebrafish. Science 345, 1358–1361.
Mecchia, M.A., Ochogavía, A., Selva, J.P., Laspina, N., Felitt, S., Martelotto, L.G., Spangenber, G., Echenique, V., Pessino, S.C., 2006. Genome polymorphisms and gene differential expression in a 'back-and-forth' ploidy-altered series of weeping lovegrass (*Eragrostis curvula*). J. Plant Physiol. 164 (8), 1051–1061.
Meyer, A., Van de Peer, Y., 2005. From 2R to 3R: evidence for a fish-specific genome duplication (FSGD). Bioessays 27 (9), 937–945.
Mitchell, L.J., Tettamanti, V., Rhodes, J.S., Marshall, N.J., Cheney, K.L., Cortesi, F., 2021. CRISPR/Cas9-mediated generation of biallelic F0 anemonefish (*Amphiprion ocellaris*) mutants. PLoS One 19 (6), e0305644.
Oetting, W.S., Fryer, J.P., King, R.A., 1998. Mutations of the human tyrosinase gene associated with tyrosinase related oculocutaneous albinism (OCA1). Hum. Mutat. 12 (6), 433–434.
Ohno, S., 1970. Evolution by Gene Duplication. Springer-Verlag, New York.
Ota, S., Hisano, Y., Ikawa, Y., Kawahara, A., 2014. Multiple genome modifications by the CRISPR/Cas9 system in zebrafish. Genes Cells 19 (7), 555–564.
Otto, S.P., 2007. The evolutionary consequences of polyploidy. Cell 131 (3), 452–462.
Pikaard, C.S., 2001. Genomic change and gene silencing in polyploids. Trends Genet. 17 (12), 675–677.
Qin, Q.B., Wang, Y.D., Wang, J., Dai, J., Xiao, J., Hu, F.Z., Luo, K., Tao, M., Zhang, C., Liu, Y., Liu, S.J., 2014. The autotetraploid fish derived from hybridization of *Carassius auratus* red var. (female) × *Megalobrama amblycephala* (male). Biol. Reprod. 91 (4), 93.
Qin, Q.Q., Huo, Y.Y., Liu, Q.E., Wang, C.Q., Zhou, Y.W., Liu, S.J., 2018. Induced gynogenesis in autotetraploids derived from *Carassius auratus* red var. (♀) × *Megalobrama amblycephala* (♂). Aquaculture 495, 710–714.
Qin, Q.B., Cao, L., Wang, Y.Y., Ren, L., Liu, Q.W., Zhou, Y.W., Wang, C.Q., Qin, H., Zhao, C., Liu, S.J., 2019a. Rapid genomic and genetic changes in the first generation of autotetraploid lineages derived from distant hybridization of *Carassius auratus* red var. (♀) × *Megalobrama amblycephala* (♂). Mar. Biotechnol. 21 (2), 139–149.
Qin, Q.B., Liu, Q.W., Wang, C.Q., Cao, L., Zhou, Y.W., Qin, H., Zhao, C., Liu, S.J., 2019b. Molecular organization and chromosomal localization analysis of 5S rDNA clusters in autotetraploids derived from *Carassius auratus* red var. (♀) × *Megalobrama amblycephala* (♂). Front. Genet. 10, 437.
Ren, L., Gao, X., Cui, J.L., Zhang, C., Dai, H., Luo, M.X., He, S.F., Qin, Q.B., Luo, K.K., Tao, M., Xiao, J., Wang, J., Zhang, H., Zhang, X.Y., Zhou, Y., Wang, J., Zhao, X., Liu, G.M., Wang, G.L., Huo, L.H., Wang, S., Hu, F.Z., Zhao, R.R., Zhou, R., Wang, Y. D., Liu, Q.F., Yan, X.J., Wu, C., Yang, C.H., Tang, C.C., Duan, W., Liu, S.J., 2022. Symmetric subgenomes and balanced homoeolog expression stabilize the establishment of allopolyploidy in cyprinid fish. BMC Biol. 20 (1), 200.
Session, A.M., Uno, Y., Kwon, T., Chapman, J.A., Toyoda, A., Takahashi, S., Fukui, A., Hikosaka, A., Suzuki, A., Kondo, M., van Heeringen, S.J., Quigley, I., Heinz, S., Ogino, H., Ochi, H., Hellsten, U., Lyons, J.B., Simakov, O., Putnam, N., Stites, J., Kuroki, Y., Tanaka, T., Michiue, T., Watanabe, M., Bogdanovic, O., Lister, R., Georgiou, G., Paranjpe, S.S., van Kruijsbergen, I., Shu, S., Carlson, J., Kinoshita, T., Ohta, Y., Mawaribuchi, S., Jenkins, J., Grimwood, J., Schmutz, J., Mitros, T., Mozaffari, S.V., Suzuki, Y., Haramoto, Y., Yamamoto, T.S., Takagi, C., Heald, R., Miller, K., Haudenschild, C., Kitzman, J., Nakayama, T., Izutsu, Y., Robert, J., Fortriede, J., Burns, K., Lotay, V., Karimi, K., Yasuoka, Y., Dichmann, D.S., Flajnik, M.F., Houston, D.W., Shendure, J., DuPasquier, L., Vize, P.D., Zorn, A.M., Ito, M., Marcotte, E.M., Wallingford, J.B., Ito, Y., Asashima, M., Ueno, N., Matsuda, Y., Veenstra, G.J., Fujiyama, A., Harland, R.M., Taira, M., Rokhsar, D.S., 2016. Genome evolution in the allotetraploid frog *Xenopus laevis*. Nature 538 (7625), 336–343.
Sheng, J.Q., Guan, L., Sheng, B., Geng, S.Y., Wu, D., Hu, B.J., Li, Z.X., Le, S.L., Hong, Y.J., 2021. Analysis of pigment cell composition, pigment content, tyrosinase content and activity of three kinds of loaches, *Misgurnus anguillicaudatus* from poyang lake. J. Fish Biol. 100 (2), 366–377.
Solano, F., 2018. On the metal cofactor in the tyrosinase family. Int. J. Mol. Sci. 19 (2), 633.
Soltis, D.E., Soltis, P.S., Tate, J.A., 2003. Advances in the study of polyploidy since plant speciation. New Phytol. 161 (1), 173–191.
Song, C., Liu, S.J., Xiao, J., He, W.G., Zhou, Y., Qin, Q.B., Zhang, C., Liu, Y., 2012. Polyploid organisms. Sci. China Life Sci. 55 (4), 301–311.
Tu, S., Johnson, S.L., 2010. Clonal analyses reveal roles of organ founding stem cells, melanocyte stem cells and melanoblasts in establishment, growth and regeneration of the adult zebrafish fin. Development 137 (23), 3931–3939.
Van de Peer, Y., Mizrachi, E., Marchal, K., 2017. The evolutionary significance of polyploidy. Nat. Rev. Genet. 18 (7), 411–424.
Wang, H.Y., Yang, H., Shivalila, C.S., Dawlaty, M.M., Cheng, A.W., Zhang, F., Jaenisch, R., 2013. One-step generation of mice carrying mutations in multiple genes by CRISPR/Cas-mediated genome engineering. Cell 153 (4), 910–918.
Wang, Y., Li, S.M., Huang, J., Chen, S.Y., Liu, Y.P., 2014. Mutations of TYR and MITF genes are associated with plumagecolour phenotypes in geese. Asian Australas. J. Anim. Sci. 27 (6), 778–783.
Wang, F., Shi, Z., Cui, Y., Guo, X.G., Shi, Y.B., Chen, Y.L., 2015. Targeted gene disruption in *Xenopus laevis* using CRISPR/Cas9. Cell Biosci. 5, 15.
Wang, S., Zhou, P., Huang, X.X., Liu, Q.L., Lin, B., Fu, Y.Q., Gu, Q.H., Hu, F.Z., Luo, K.K., Zhang, C., Tao, M., Qin, Q.B., Liu, S.J., 2020a. The establishment of an autotetraploid fish lineage produced by female allotetraploid hybrids × male homodiploid hybrids derived from *Cyprinus carpio* (♀) × *Megalobrama amblycephala* (♂). Aquaculture 515, 734583.
Wang, C.Q., Zhou, Y.W., Qin, H., Zhao, C., Yang, L., Yu, T.T., Zhang, Y.X., Xu, T., Qin, Q. B., Liu, S.J., 2020b. Genetic and epigenetic changes are rapid responses of the genome to the newly synthesized autotetraploid *Carassius auratus*. Front. Genet. 11, 576260.
Wang, C.Q., Qin, H., Zhao, C., Yang, L., Yu, T.T., Zhang, Y.X., Luo, X., Qin, Q.B., Liu, S.J., 2021. Whole-genome re-sequencing and transcriptome reveal oogenesis-related genes in autotetraploid *Carassius auratus*. Mar. Biotechnol. 23 (2), 233–241.
Xu, P., Zhang, X.F., Wang, X.M., Li, J.T., Liu, G.M., Kuang, Y.Y., Xu, J., Zheng, X.H., Ren, L.F., Wang, G.L., Zhang, Y., Huo, L.H., Zhao, Z.X., Cao, D.C., Lu, C.Y., Li, C., Zhou, Y., Liu, Z.J., Fan, Z.H., Shan, G.L., Li, X.G., Wu, S.X., Song, L.P., Hou, G.Y., Jiang, Y.L., Jeney, Z., Yu, D., Wang, L., Shao, C.J., Song, L., Sun, J., Ji, P.F., Wang, J., Li, Q., Xu, L.M., Sun, F.Y., Feng, J.X., Wang, C.H., Wang, S.L., Wang, B.S., Li, Y., Zhu, Y.P., Xue, W., Zhao, L., Wang, J.Y., Gu, Y., Lv, W.H., Wu, K.J., Xiao, J.F., Wu, J. Y., Zhang, Z., Yu, J., Sun, X.W., 2014. Genome sequence and genetic diversity of the common carp, *Cyprinus carpio*. Nat. Genet. 46 (11), 1212–1219.
Xu, X.W., Cao, X.J., Gao, J., 2019a. Production of a mutant of large-scale loach *Paramisgurnus dabryanus* with skin pigmentation loss by genome editing with CRISPR/Cas9 system. Transgenic Res. 28 (3–4), 341–356.
Xu, P., Xu, J., Liu, G.J., Chen, L., Zhou, Z.X., Peng, W.Z., Jiang, Y.L., Zhao, Z.X., Jia, Z.Y., Sun, Y.H., Wu, Y.D., Chen, B.H., Pu, F., Feng, J.X., Luo, J., Chai, J., Zhang, H.Y., Wang, H., Dong, C.J., Jiang, W.K., Sun, X.W., 2019b. The allotetraploid origin and asymmetrical genome evolution of the common carp *Cyprinus carpio*. Nat. Commun. 10 (1), 4625.
Xu, X.D., Chen, H.L., Mandal, B.K., Si, Z.X., Wang, J., Wang, C.H., 2022. Duplicated *Tyr* disruption using CRISPR/Cas9 reveals melanophore formation in Oujiang color common carp (*Cyprinus carpio* var. *color*). Reprod. Breed. 2 (2), 37–45.
Xu, X.D., Wang, C.Q., Xiao, Q.W., Huang, X., Zhou, Y., Luo, X., Zhang, Y.X., Xu, X.W., Qin, Q.B., Liu, S.J., 2023. The alternative transcription and expression characterization of *Dmc1* in autotetraploid *Carassius auratus*. Front. Genet. 14, 1135006.
Xu, X.D., Zhou, Y., Wang, C.Q., Huang, X., Zhang, K., Xu, X.W., He, L.W., Zhang, X.Y., Fu, X.Z., Ma, M., Qin, Q.B., Liu, S.J., 2024. Identification and effective regulation of *scarb1* gene involved in pigmentation change in autotetraploid *Carassius auratus*. Zool. Res. 45 (2), 381–397.
Zhang, X.T., Wei, K.J., Chen, Y.Y., Shi, C.C., Liu, L.K., Li, J., Zhang, Z.R., Ji, W., 2018. Molecular cloning and expression analysis of *Tyr* and *Tyrp1* genes in normal and albino yellow catfish *Tachysurus fulvidraco*. J. Fish Biol. 92 (4), 979–998.
Zhou, L., Gui, J., 2017. Natural and artificial polyploids in aquaculture. Aquacult. Fish. 2 (3), 103–111.
Zhu, Y., Xiao, W., 2004. Pdr3 is required for DNA damage induction of *MAG1* and *DDI1* via a bi-directional promoter element. Nucleic Acids Res. 32 (17), 5066–5075.
Zhu, Z., Tian, N.N., Yang, R.B., Yang, X.F., 2022. Distribution and comparison of melanin in different tissues and organs of *Triplophysa stenura* and *T.Orientalis*. Ying Yong Sheng Tai Xue Bao 33 (12), 3410–3418.